



Review

Arc-Induced Long-Period Fiber Gratings at INESC TEC. Part II: Properties and Applications in Optical Communications and Sensing

Gaspar Rego ^{1,2,*} , Paulo Caldas ^{1,2}  and Oleg V. Ivanov ^{3,4}

¹ ProMetheus, Instituto Politécnico de Viana do Castelo, Rua Escola Industrial e Comercial Nun'Álvares, 4900-347 Viana do Castelo, Portugal; pcaldas@estg.ipvc.pt

² Center for Applied Photonics, INESC TEC, Rua Dr. Roberto Frias, 4200-465 Porto, Portugal

³ Ulyanovsk Branch of Kotel'nikov Institute of Radio Engineering and Electronics of Russian Academy of Sciences, Ulitsa Goncharova 48, 432071 Ulyanovsk, Russia; olegivvit@yandex.ru

⁴ Ulyanovsk State University, Ulitsa L. Tolstogo 42, 432017 Ulyanovsk, Russia

* Correspondence: gaspar@estg.ipvc.pt

Abstract: In this work, we review the most important achievements of INESC TEC related to the properties and applications of arc-induced long-period fiber gratings. The polarization dependence loss, the spectral behavior at temperatures ranging from cryogenic up to 1200 °C and under exposure to ultraviolet and gamma radiation is described. The dependence of gratings sensitivity on the fabrication parameters is discussed. Several applications in optical communications and sensing domains are referred.

Keywords: long-period fiber grating; arc-induced fiber grating; optical communications; optical fiber sensor



Citation: Rego, G.; Caldas, P.; Ivanov, O.V. Arc-Induced Long-Period Fiber Gratings at INESC TEC. Part II: Properties and Applications in Optical Communications and Sensing. *Sensors* **2021**, *21*, 5914. <https://doi.org/10.3390/s21175914>

Academic Editor: Andrea Cusano

Received: 23 July 2021

Accepted: 30 August 2021

Published: 2 September 2021

Publisher's Note: MDPI stays neutral with regard to jurisdictional claims in published maps and institutional affiliations.



Copyright: © 2021 by the authors. Licensee MDPI, Basel, Switzerland. This article is an open access article distributed under the terms and conditions of the Creative Commons Attribution (CC BY) license (<https://creativecommons.org/licenses/by/4.0/>).

1. Introduction

Long-period fiber gratings (LPFGs) exhibit resonances at specific wavelengths as a result of coupling of the core mode to discrete cladding modes and can work as wavelength selective optical filters. Therefore, LPFGs find application in the optical communications domain as band rejection filters. They have been used or proposed for a number of applications such as gain equalization in erbium doped fiber amplifiers, elimination of Stokes orders in cascaded Raman amplifiers/lasers, suppression of the stimulated Raman scattering in MOPA fiber laser and the amplified spontaneous emission [1–8]. They have also been used for temperature stabilization of Er-doped superfluorescent fiber sources [9]. The gratings' rejection bands can be made very broad [10] being useful for polarization dependent loss compensation. Ultimately, they can be made wavelength independent and, consequently, can act as variable optical attenuators [11]. On the other hand, by cascading two identical gratings it is possible to obtain very narrow optical filters [12–14] being, therefore, useful devices in wavelength division multiplexing and optical code division multiple access systems [15,16]. The use of LPFGs for dark hollow beam generator [17], or as mode converters in standard fibers [18], two-mode fibers [19,20] and as wavelength selective polarizers [21–26] has also been demonstrated. LPFGs can be used to enhance coupling between fiber and a waveguide [27], a semiconductor laser or a bulk optical element [28]. Coupling between a fiber and the free space by producing a planar wave was also demonstrated [29]. Two important applications of LPFGs in optical communications such as optical switches [30–32] and add-drop multiplexers can be realized by using two gratings in close proximity [33], a grating assisted fiber coupler [34] or coupling between mismatched twin-core fibers [35]. LPFGs can act as ultrafast optical differentiators [36]. The use of LPFGs as dispersion compensators has also been investigated theoretically [37–39]. LPFGs alone or with other gratings have been used for producing

multiwavelength fiber lasers [39–43] or simply a more stable fiber laser output [44]. LPFGs can also act as bandpass filters by using phase-shifted gratings [45,46] or two concatenated gratings with a core-mode blocker in between [47–50].

Long period fiber gratings are very sensitive to changes in physical parameters, such as, temperature [51], strain [52,53], transverse load [54], bending [55], torsion [56] and refractive index of the surrounding medium [57–59] and, therefore, several sensor heads have been proposed to monitor temperature in extreme environments [60,61], structural integrity [62], multi-directional bending [63] and torsion [64]. On the other hand, coated LPFGs [65–67] can act as refractometric sensors [68,69] able to monitor an enormous quantity of physical [70–72], chemical [73–75] and biological parameters [76–80].

In the following sections we will present the properties of arc-induced gratings and discuss several applications in the sensing field. Since one of the first identified advantages of LPFGs produced by using the electric arc technique is their stability at high temperatures, we begin by presenting a detailed study on the thermal behavior of these gratings. Thus, we introduce the equations related to the determination of gratings sensitivity, followed by the thermal behavior up to 1200 °C, the effect of the heating cycles namely on the strain point, the study of the stability at high temperatures over time and finally their behavior at cryogenic temperatures. In the third section we discuss the influence of the fabrication parameters on the temperature and strain sensitivity, followed by their sensitivity to other physical parameters such as, bending and surrounding refractive index. Afterwards, we present an important characteristic of arc-induced gratings: they intrinsically exhibit high polarization dependence loss (PDL) [81], which in fact imposes limitations on their use in the optical communications domain. On the other hand, this property also enables their use as a sensor for the simultaneous measurement of temperature and strain [82]. The section ends by showing the effect of LPFGs exposure to uniform uv-radiation and gamma radiation. The first gives information related to the mechanisms of gratings formation and the second related to the possibility of using sensors, based on arc-induced gratings, in extreme environments. The fourth section is concerned to the study of three sensor heads that allow for the simultaneous measurement of temperature and strain, that overcome cross-sensitivity and finally an original flow sensor is also presented.

2. Thermal Behavior of Arc-Induced Gratings

Among the different physical parameters that gratings can be used to monitor, temperature is one of the most important. Therefore, a detailed analysis on their thermal behavior will be presented ranging from cryogenic up to very high temperatures. Naturally, the behavior depends on the fiber itself.

2.1. Theoretical Equations Concerning the Gratings Sensitivity

For an LPFG, the wavelength at which the mode coupling occurs is given by [83]:

$$\lambda_{res} = \left(n_{co}^{eff} - n_{cl,m}^{eff} \right) \Lambda \quad (1)$$

where λ_{res} represents the resonance wavelengths, Λ is the grating period and n_{co}^{eff} and $n_{cl,m}^{eff}$ are the effective refractive indices of the core mode and the m -th cladding mode, respectively.

The temperature sensitivity of an LPFG is expressed by the following equations [84]:

$$\frac{d\lambda_{res}}{dT} = \lambda_{res} \gamma (\alpha + \Gamma_{Temp}) \quad (2)$$

where α is the thermal expansion coefficient of the fiber. γ , the general sensitivity factor, describes the waveguide dispersion and is expressed by:

$$\gamma = \frac{\frac{d\lambda_{res}}{d\Lambda}}{n_{co}^{eff} - n_{cl,m}^{eff}} \quad (3)$$

where $d\lambda_{res}/d\Lambda$ represents the slope of the dispersion curves. Γ_{Temp} describes the temperature dependence of the waveguide dispersion and is expressed by:

$$\Gamma_{Temp} = \frac{\xi_{co}n_{co}^{eff} - \xi_{cl}n_{cl,m}^{eff}}{n_{co}^{eff} - n_{cl,m}^{eff}} \quad (4)$$

where ξ_{co} and ξ_{cl} are the thermo-optic coefficients of the core and cladding materials. Analogously, the strain sensitivity can be expressed by:

$$\frac{d\lambda_{res}}{d\varepsilon} = \lambda_{res}\gamma(1 + \Gamma_{strain}) \quad (5)$$

Γ_{strain} describes the strain dependence of the waveguide dispersion and is expressed by:

$$\Gamma_{strain} = \frac{\eta_{co}n_{co}^{eff} - \eta_{cl}n_{cl,m}^{eff}}{n_{co}^{eff} - n_{cl,m}^{eff}} \quad (6)$$

where η_{co} and η_{cl} are the elasto-optic coefficients of the core and cladding materials.

In which concerns the surrounding refractive index sensitivity, the following equations apply:

$$\frac{d\lambda_{res}}{dn_{surr}} = \lambda_{res}\gamma\Gamma_{surr} \quad (7)$$

where Γ_{surr} is expressed by:

$$\Gamma_{surr} = - \frac{u_m^2 \lambda_{res}^3 n_{surr}}{8\pi r_{cl}^3 n_{cl} (n_{co}^{eff} - n_{cl,m}^{eff}) (n_{cl}^2 - n_{surr}^2)^{3/2}} \quad (\text{valid for } n_{surr} < n_{cl}) \quad (8)$$

and describes the dependence of the waveguide dispersion on the surrounding refractive index (n_{surr}). The term u_m is the m -th root of the zero-order Bessel function and the other symbols have their common meaning. A discussion on the ways to increase the LPFGs sensitivity to changes on the surrounding refractive index was presented in [68]. The analysis of the above equations enables one to conclude that changes to the effective refractive indices of core and cladding will impact the gratings sensitivities. In particular, as will be shown below, since the arc discharge affects not only the fiber cross section but also changes the strains in the fiber core and cladding it is expected that the temperature and strain sensitivity may be tuned by adjusting the fabrication parameters.

2.2. LPFGs' Temperature Sensitivity from Room Temperature up to 1200 °C

First, we present the behavior from room temperature up to 1200 °C for gratings arc-induced in different type of fibers and afterwards we will present the behavior at cryogenic temperatures.

In order to investigate the gratings thermal behavior, they were placed inside a tubular oven and a weight was applied to keep the fiber straight. The temperature was raised from room temperature up to about 1000 °C in steps of typically 50 °C. At each step the temperature was kept constant for about 10 min in order to the fiber reach thermal equilibrium. Figure 1 shows the general behavior for a 540 μm LPFG written in the Siacor fiber. As it can be seen the resonance wavelengths shift non-linearly towards longer wavelengths as the temperature increases. The temperature sensitivity increases with the

order of the cladding mode resonances and also with the temperature increase except around the strain point.

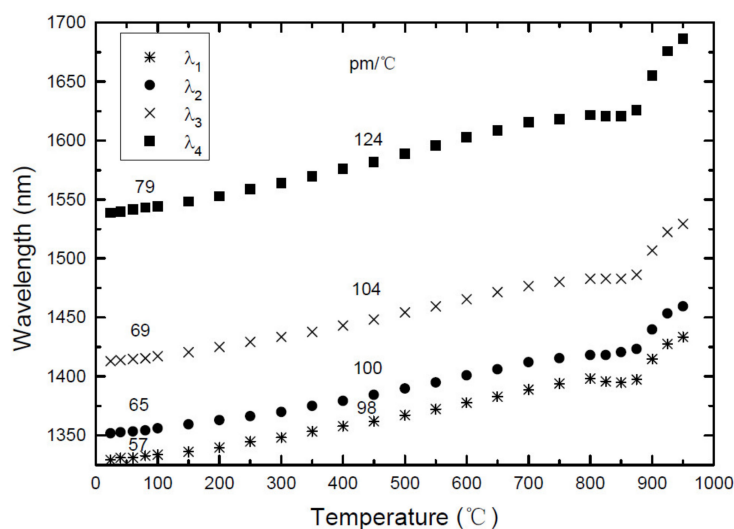


Figure 1. Thermal behavior of a 540 μm LPFG arc-induced in the Siorc fiber. Reprinted with permission from ref. [85]. © 2021 Taylor and Francis.

The thermal behavior of LPFGs arc-induced in Ge-doped fibers and in Ge-free fibers is presented in Figures 2 and 3, respectively. In general, for Ge-doped fibers the resonance wavelengths shift quadratically with the temperature increase from room temperature up to the strain point. At this point, typically around 700 $^{\circ}\text{C}$, the glass structure starts to relax and depending on the fiber composition and fabrication history (drawing temperature and tension) the resonance wavelengths show different behaviors, that is, the slope decreases or even become negative as will be discussed below. For the B/Ge co-doped fiber the resonance wavelengths shift towards shorter wavelengths up to 300–400 $^{\circ}\text{C}$ and afterwards to longer wavelengths. This is a consequence of the presence of B_2O_3 that decreases the thermo-optic coefficient in comparison to the one of SiO_2 and GeO_2 . Afterwards, the slope becomes more pronounced due to the thermal expansion of glass, since its contribution becomes comparable to the dependence of the refractive index on temperature.

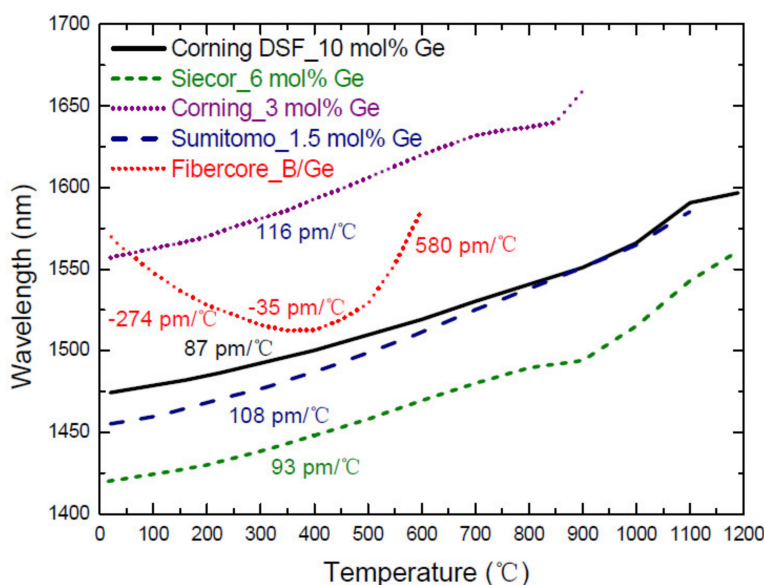


Figure 2. Thermal behavior of LPFGs arc-induced in Ge-doped fibers. Reprinted from [86].

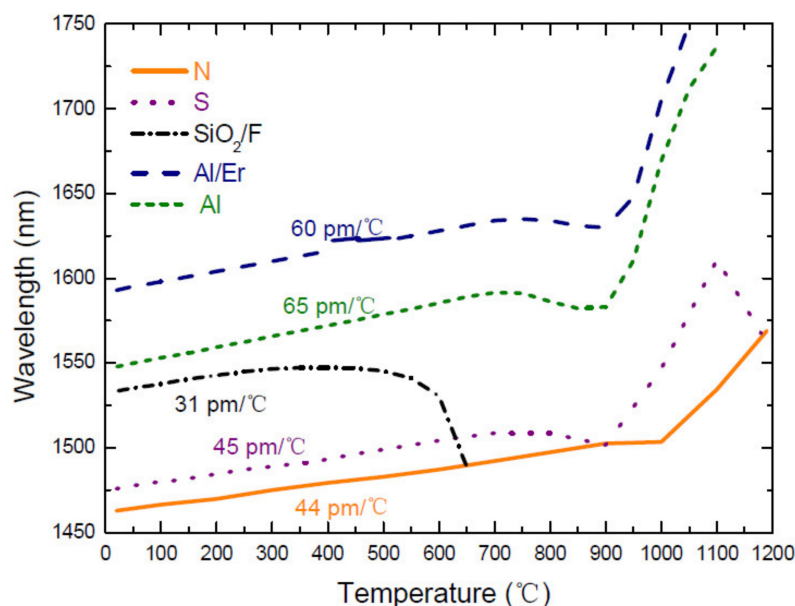


Figure 3. Thermal behavior of LPFGs arc-induced in Ge-free fibers. Reprinted from [86].

The major difference between these two figures is that the temperature sensitivity is constant for Ge-free fibers while it shows a linear dependence for Ge-doped fibers. This behavior becomes more evident in Figure 4. Table 1 summarizes the temperature sensitivities obtained for gratings inscribed in different fibers. Thermal studies below 200 °C were also conducted in Ge-free fibers by S. Campopiano et al. [87–89]. In the case of pure-silica core fibers and Er doped fibers similar results were obtained. For gratings inscribed in a P-doped fiber, values for the temperature sensitivity ranging from -58 to -116 pm/°C were obtained (also temperature dependent) for two distinct grating periods and cladding mode orders.

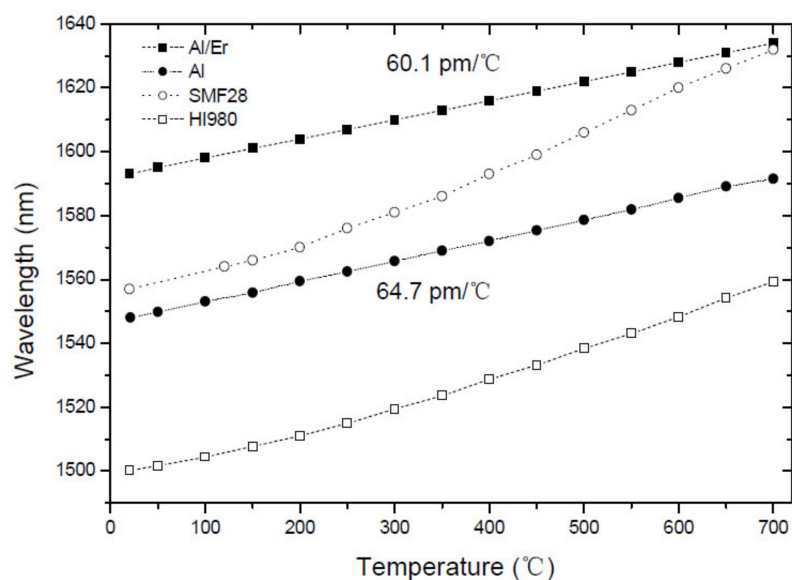


Figure 4. Comparison of the thermal behavior of LPFGs arc-induced in Ge-doped and in aluminosilicate fibers. Reprinted from [86].

Table 1. Temperature sensitivity of gratings written in different fibers. Adapted from [86].

Fiber (mol% GeO ₂)	D _{core} /μm	Λ/μm	Mode Order	Temperature Sensitivity (pm °C ⁻¹)
Sumitomo_1.5	8.3	540	4	58.1 + 0.125 T
SMF-28_3	8.6	540	4	72.3 + 0.12 T
Siecor_6	8.3	540	4	76.7 + 0.11 T
HI-980	~4	540	5	56.2 + 0.09 T
Corning_DSF_12	5.1	540	3	39.4 + 0.13 T
Al	4.25	400	4	64.7 T ≤ 700
Al/Er	4.55	400	4	60.1 T ≤ 700
S	not available	540	4	50 T ≤ 700
Oxford_SiO ₂ /F	9	730	2	47.1 T ≤ 300
ACREO_SiO ₂ /F	not available	730	3	40.1 T ≤ 300
N'94	2	240	6	45 T ≤ 900
N'96	4.5	540	5	43 T ≤ 900
N1905	6.2	400	4	67 T ≤ 400
N1940	5.8	400	4	51.9 T ≤ 400

2.3. Heating Cycles and Strain Point

The thermal behavior can be modified by submitting the LPFGs to heating cycles. One grating (fabrication parameters: 5.1 g, 9 mA, 1 s, 40) was heated from room temperature up to 900 °C four times and as Figure 5 shows after the third annealing the fiber was in thermal equilibrium (the fourth cycle retraces the third one). As it can be seen, comparatively to the first heating cycle the whole spectrum shifted towards longer wavelengths and the stress relaxation region vanished. The figure also shows the annealing of a second similar grating, but this time the grating was heated up to 700 °C and was kept at that temperature for 15 h. It was observed that the LP₁₃ cladding mode shifted 18 nm towards shorter wavelengths (LP₁₄ shifted 25 nm). It should be stressed that the LPFGs fabrication parameters may have some influence on this behavior since a third grating (1.1 g, 12 mA, 0.5 s, 40) shown a down shift of 55 nm. Moreover, detailed studies were presented by Humbert et al. [90,91] in the 700–800 °C temperature range concerning gratings fabricated with no use of external tension and exhibited lower wavelength shifts. After cooling down the second grating to room temperature, it was submitted to an annealing temperature of 800 °C for 6 h. This time the spectrum moved 55 nm towards longer wavelengths. This may reflect a rearrangement of the glass structure towards a new thermodynamic equilibrium as a consequence of the interplay between stress relaxation and the fiber thermal expansion coefficients and viscosities, which are also time and temperature dependent.

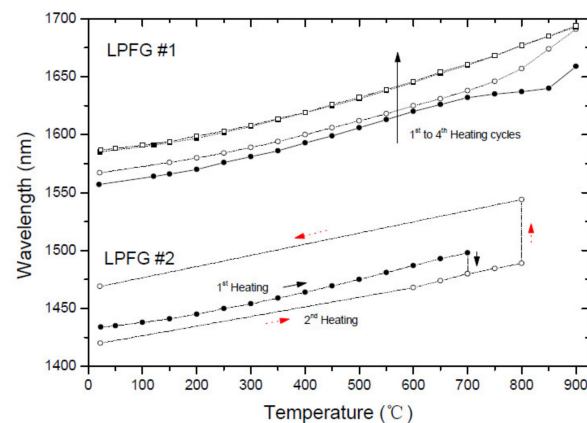


Figure 5. Thermal behavior of LPFGs submitted to several heating cycles. Adapted with permission from ref. [85]. © 2021 Taylor and Francis.

Stress relaxations in the 700–800 °C temperature range was first observed in [92]. Figure 6 shows the movement of two resonances belonging to a LPFG (22.8 g, 9 mA, 1 s, 40) during the annealing at 800 °C for 6 h. As it can be observed, the resonances move first towards shorter wavelengths and afterwards towards longer wavelengths where they stabilize, being the shift larger for the highest order cladding mode.

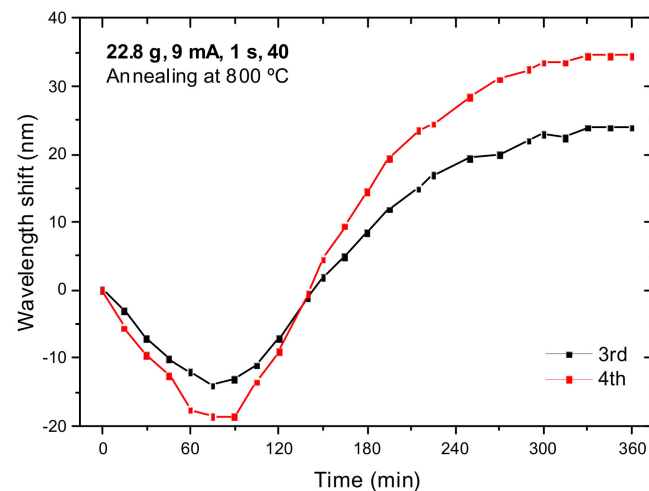


Figure 6. Time dependence of two resonances during annealing at 800 °C for 6 h. Reprinted from [86].

However, stress relaxations can occur at much lower temperatures, around 300 °C as was found for pure-silica-core fibers and for the FiberCore B/Ge co-doped fiber [93,94]. Relaxations at about 400 °C were also found in elongation experiments with several types of fiber drawn with different drawing tensions [95]. Figure 7 shows the thermal behavior of LP₀₅ cladding mode belonging to a LPFG (5.1 g, 9 mA, 0.5 s, 400 μm, 60) arc-induced in the B/Ge co-doped fiber. A minute change can be detected at 300 °C but it increases at higher temperatures. After cooling down the LPFG from temperatures in the range of 300–700 °C, the LP₀₅ cladding mode shifted to longer wavelengths by 2, 12, 50, 203 and 249 nm, respectively. It should be noted that the erasure of the grating started for temperatures above 700 °C, being completely eliminated after 25 min at 800 °C.

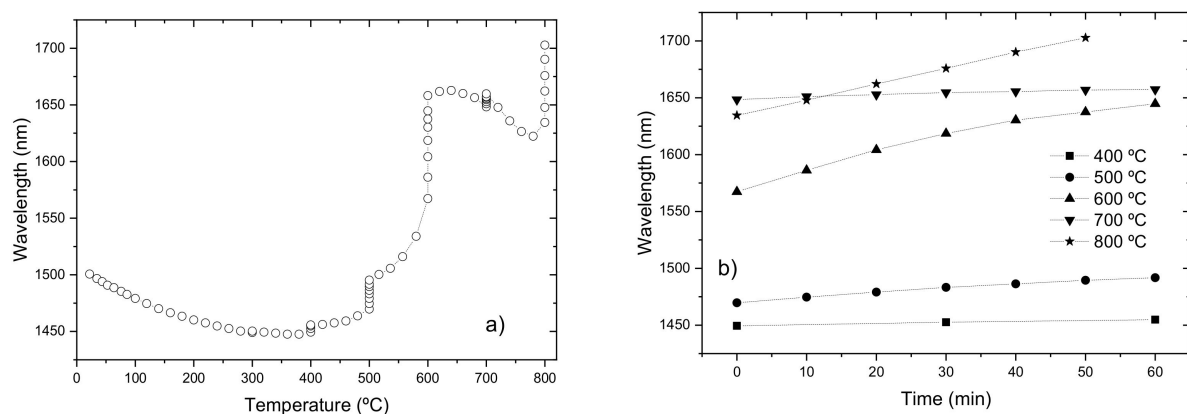


Figure 7. (a,b) Heating cycle up to 800 °C with dwell time of 1 h at each step. Reprinted with permission from ref. [96]. © 2021 Wiley Periodicals, Inc.

2.4. LPFGs' Stability at High Temperatures

The thermal annealing of several gratings, inscribed in different type of fibers, at high temperatures was also investigated [97]. Figure 8 shows the wavelength shift during annealing performed at 1000 °C during 24 h. It is interesting to note that gratings inscribed

in germanium doped fibers move towards longer wavelengths, while gratings inscribed in germanium free fibers (pure-silica-core and nitrogen doped fibers) the shift is much larger and is precisely in the opposite direction. There is no clear understanding of the reasons for this behavior. The standard fibers appear to approach an equilibrium situation, after a process of stress relaxation and thermal expansion, whilst for the other fibers diffusion and chemical processes might be involved leading to a degradation of the pristine fiber. As shown in Figure 9, gratings annealed at 1000 °C for 1 day exhibits some degree of degradation. A similar study was conducted by Morishita et al. [98] in the Corning SMF28 fiber. The shifts obtained are larger which might be due to the higher arc currents used in their work. It should be stressed that annealing at higher temperatures for a couple of hours wash out the grating (1100 °C) [98] followed by a degradation of the fiber itself (1200 °C, the annealing temperature approaches the fiber fictive temperature) [92].

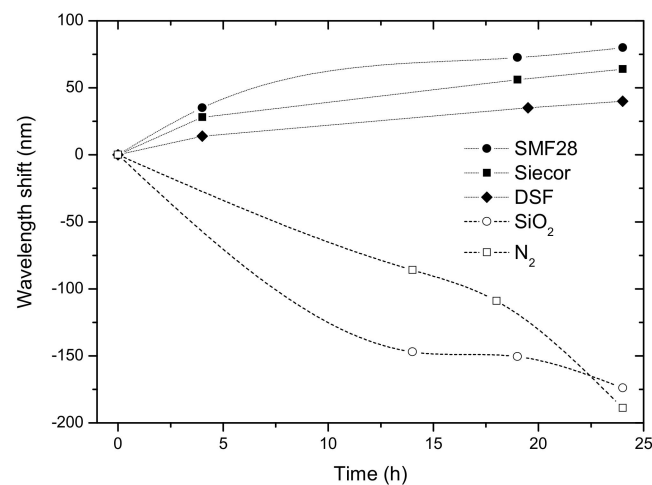


Figure 8. Time dependence of the resonant wavelength at 1000 °C. Reprinted with permission from ref. [97]. © 2021 IEE.

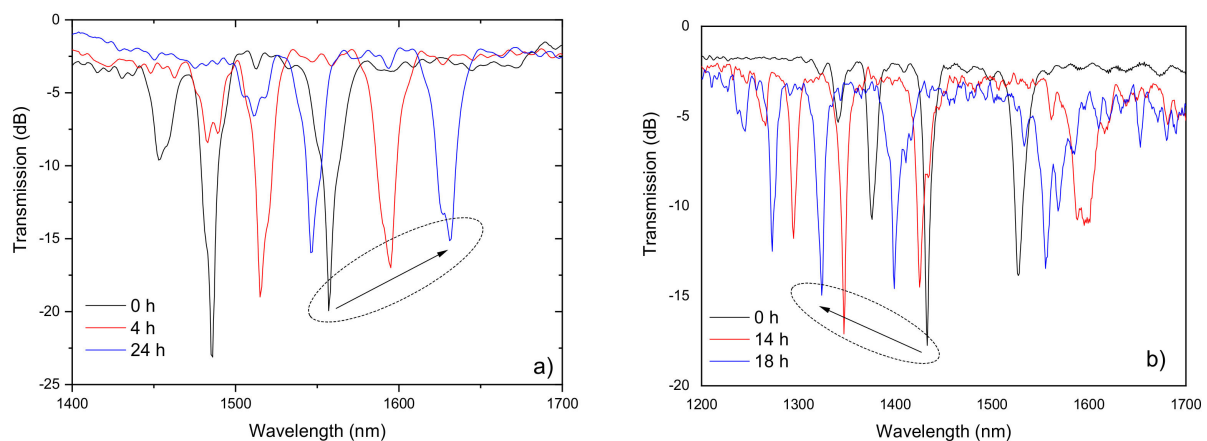


Figure 9. Evolution of the spectra of two gratings written in the (a) SMF28 fiber; and in a (b) nitrogen doped fiber during annealing at 1000 °C. Adapted with permission from ref. [97]. © 2021 IEE.

Figure 10 shows the evolution of the transmission spectra of a grating inscribed in the Corning DSF fiber during annealing at 1190 °C for 1 h [92]. The grating withstood 30 min with only minor changes, but it was erased after 1 h. The degradation has been related to the deformation of the fiber caused by the applied external tension (5.1 g) while the fiber was heated to a temperature in the limit of the softening range. In fact, it was later measured an elongation rate of ~6 mm/min for a 180 mm long SMF-28 fiber at 1300 °C under a tension of only 1.1 g.

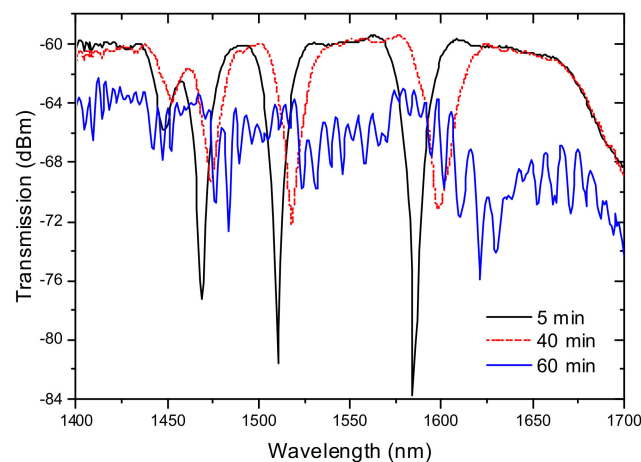


Figure 10. Annealing at 1190 °C of a 430 μm LPFG inscribed in the Corning DSF fiber. Reprinted from [86].

A study on the long time, two weeks, annealing at 1000 °C was also conducted for a LPFG (5.1 g, 9 mA, 1 s, 540 μm , 40) inscribed in the SMF28 fiber [99]. It was observed a shift of the grating spectrum to longer wavelengths and a decrease of the resonances amplitude as a result of structural relaxations. For times longer than 200 h, it was found an increase of the background loss in the transmission spectrum and the appearance of the irregular wavelength dependence, which may be due to crystallization (Figure 11).

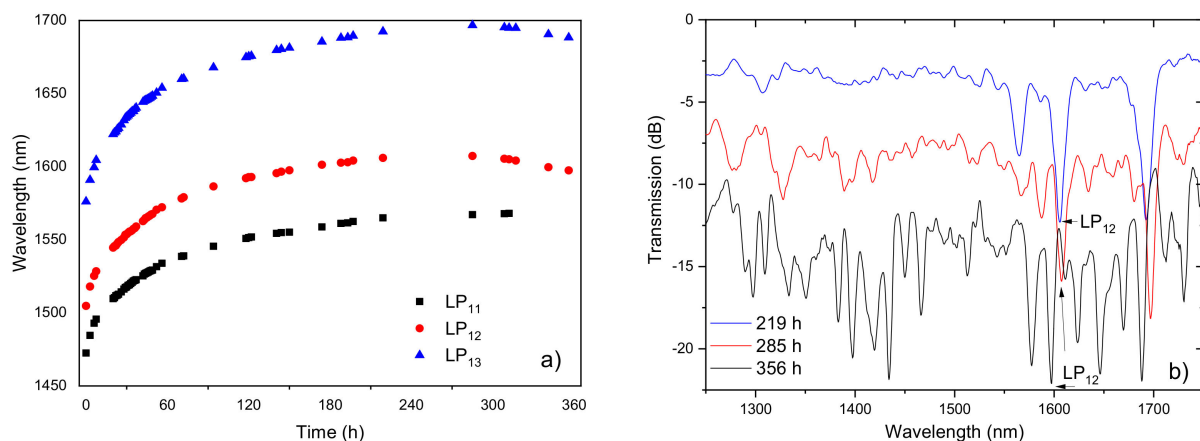


Figure 11. (a) Time dependence of the resonance wavelengths of three cladding modes and (b) evolution of the grating spectrum during the heat treatment at 1000 °C for two weeks. Adapted with permission from ref. [99]. © 2021 Elsevier.

In conclusion, the use of arc-induced gratings as high temperature sensors requires proper annealing at a temperature (higher than the strain point) above the working temperature to avoid thermal hysteresis. For temperatures as high as 1000 °C, it should be avoiding the use of external pulling tensions to keep the fiber straight since it causes fiber elongation. For example, the fiber can instead, be inserted in a closed silica capillary, this would also mitigate the effect of devitrification that can be initiated by the presence of water vapor and oxygen at such high temperatures. In any case, its use should be limited in time since degradation of the waveguide conditions will occur in the limit, due to core dopants diffusion. Thus, the implementation of high temperature optical fiber sensors requires more stable materials such as sapphire.

2.5. LPFGs at Cryogenic Temperatures

As important as the development of high temperature sensors is the development of sensors for cryogenic temperatures. We have investigated the thermal behavior of

gratings arc-induced in the SMF28 fiber and also in the B/Ge co-doped fiber at cryogenic temperatures [100]. We concluded that the temperature sensitivity of gratings inscribed in the latter fiber is considerably higher. Our results are better than the ones obtained for fiber Bragg gratings, even for those embedded/bonded to substrates with very different thermal expansion coefficients and compares well with former works also using transmissive LPFGs in this kind of fiber [101,102]. Our phase-shifted LPFG works in reflection (the fiber was cleaved and polished near the grating and uses the Fresnel reflection of the end face) being an advantage for the implementation of practical sensors for extreme environments since it only requires access to one end of the fiber. Figure 12 shows the thermal behavior of the PS-LPFG from 5 K up to room temperature for two sets of experiments. The average temperature sensitivity obtained was -0.43 nm/K in the 60–240 K range. Values ranging from -0.08 nm/K up to 0.2 nm/K were obtained in the 5–35 K temperature range. Further studies are nevertheless required to understand the behavior at low temperatures.

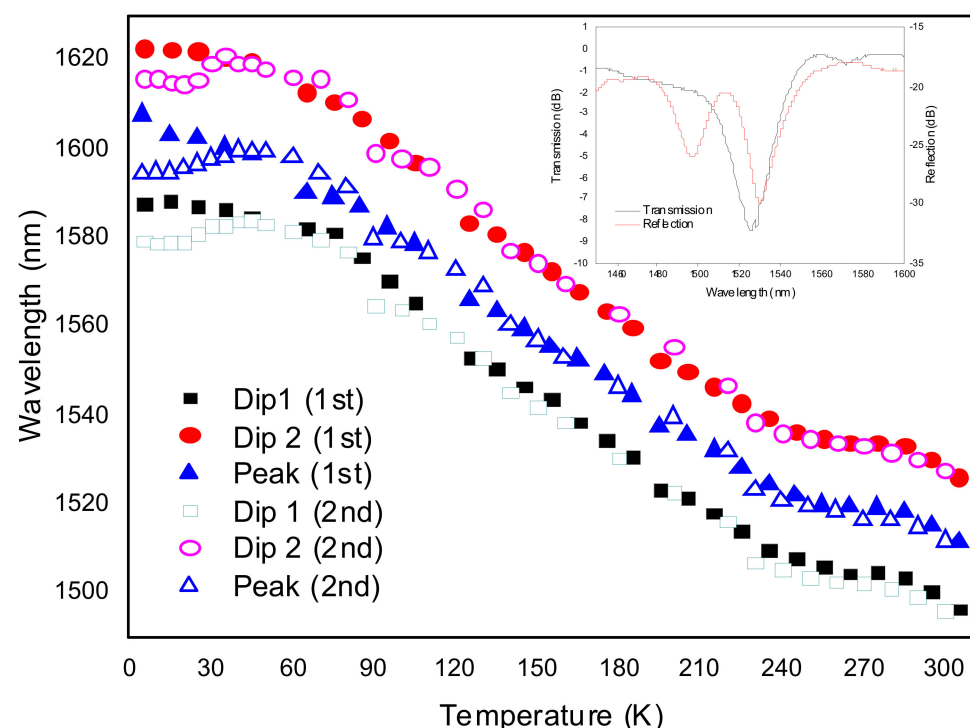


Figure 12. Wavelength of the two Dips and the Peak of the PS-LPFG, inscribed in the B/Ge co-doped fiber, as a function of temperature. Inset: PS-LPFG reflection spectrum. Adapted with permission from ref. [100]. © 2021 IEEE.

3. LPFGs' Sensitivity to Fabrication and Physical Parameters

3.1. Influence of the Fabrication Parameters on the Gratings Sensitivity

It is well-known that the sensitivity of long period gratings to changes in physical properties such as, temperature, strain and refractive index of the surrounding medium depends on the order of the cladding mode involved in the coupling [51,84,86]. This is a consequence of the dependence of the sensitivity equations on the slope of the matching curves for a particular resonance wavelength [84]. However, it was observed that changes in the fabrication parameters not only affect the position of the resonance wavelengths but also impact their sensitivities [103]. Figure 13a,b show the influence of the electric current and of the external pulling tension on the sensitivity to strain and temperature, respectively, of the LP₁₄ cladding mode belonging to a 540 μ m grating. It should be stressed that no systematic study was published so far. However, the obtained results demonstrate the ability to tune the strain and temperature sensitivity by 400% and 25%, respectively.

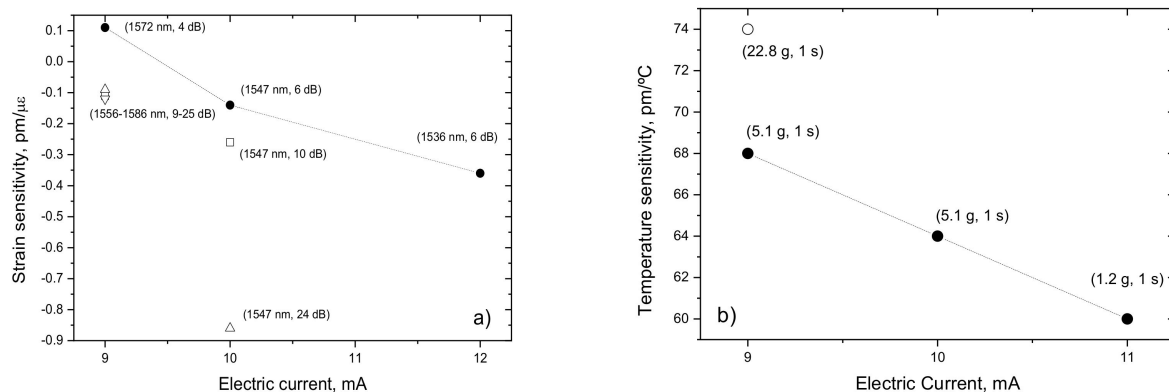


Figure 13. (a) Strain and (b) temperature sensitivity of LP₁₄ for different values of electric current and external pulling tension. Reprinted with permission from ref. [103]. © 2021 IEE.

As discussed previously [104], depending on the value of the external pulling tension, the arc discharge can release or create new stresses in the optical fiber. It can also induce microdeformations in the fiber cross section. Therefore, the geometric and the structural changes will impact the effective refractive indexes of core and cladding modes and thus, from Equations (1)–(6), the grating sensitivity to both strain and temperature.

3.2. Sensitivity to Other Physical Parameters

LPGs are sensitive to other parameters such as strain [105–108], bending [109–111], torsion [112–114], pressure [115,116] and surrounding refractive index [89,117–124]. On contrary to what happens for the temperature sensitivity, the strain sensitivity is typically an order of magnitude lower than for FBGs. As discussed above, besides the order of the cladding mode the sensitivity increases with the decrease of the fiber cross section. However, a LPFG (36.3 g, 9 mA, 0.5 s, 730 μm , 75) inscribed in a pure silica core fiber exhibited a strain sensitivity of $-1.4 \text{ pm}/\mu\epsilon$ (Figure 14a) [94] which compares well with the values obtained for FBGs and is also larger than the typical values shown in Figure 13. On the other hand, LPFGs are very sensitive to bending what is a considerable drawback when one wants to measure parameters other than curvature. Even though LPFGs can be used for bending [109] (Figure 14b), a Mach-Zehnder configuration comprising two LPFGs separated by 15 cm was used for refractive index measurement and it was demonstrated that the sensitivity can be improved if one bent the region in between the gratings [125]. LPFGs are also sensitive to the external refractive index and therefore they can be used as a liquid level sensor or a refractometric sensor [68,119]. Figure 14c present results on the behavior of a Michelson interferometer when different lengths of the cavity are immersed in water. The sensor sensitivity increases with the length of the cavity, the order of the cladding modes and also with the decrease of the cladding diameter [126]. Figure 14d presents the displacement of the resonance peaks as a function of the external refractive index for aqueous solutions. A sensitivity as high as $-0.7 \mu\text{m}/\text{RIU}$ @1.33 was obtained for a 192 μm -LPFG near the turning points, inscribed in a B/Ge co-doped fiber [127]. The sensitivity can exceed 1.3 $\mu\text{m}/\text{RIU}$ if the dual resonances are considered. These values are at least 20 times higher than the ones presented in [118]. In this context, further improvements have been achieved when gratings were inscribed in etched cladding fibers [122] and/or fibers were coated with thin films [79,128–136]. L. Coelho et al. at INESC TEC conducted relevant research related to the influence of metal oxide coating on arc-induced gratings and their applications as refractometric sensors [137–145].

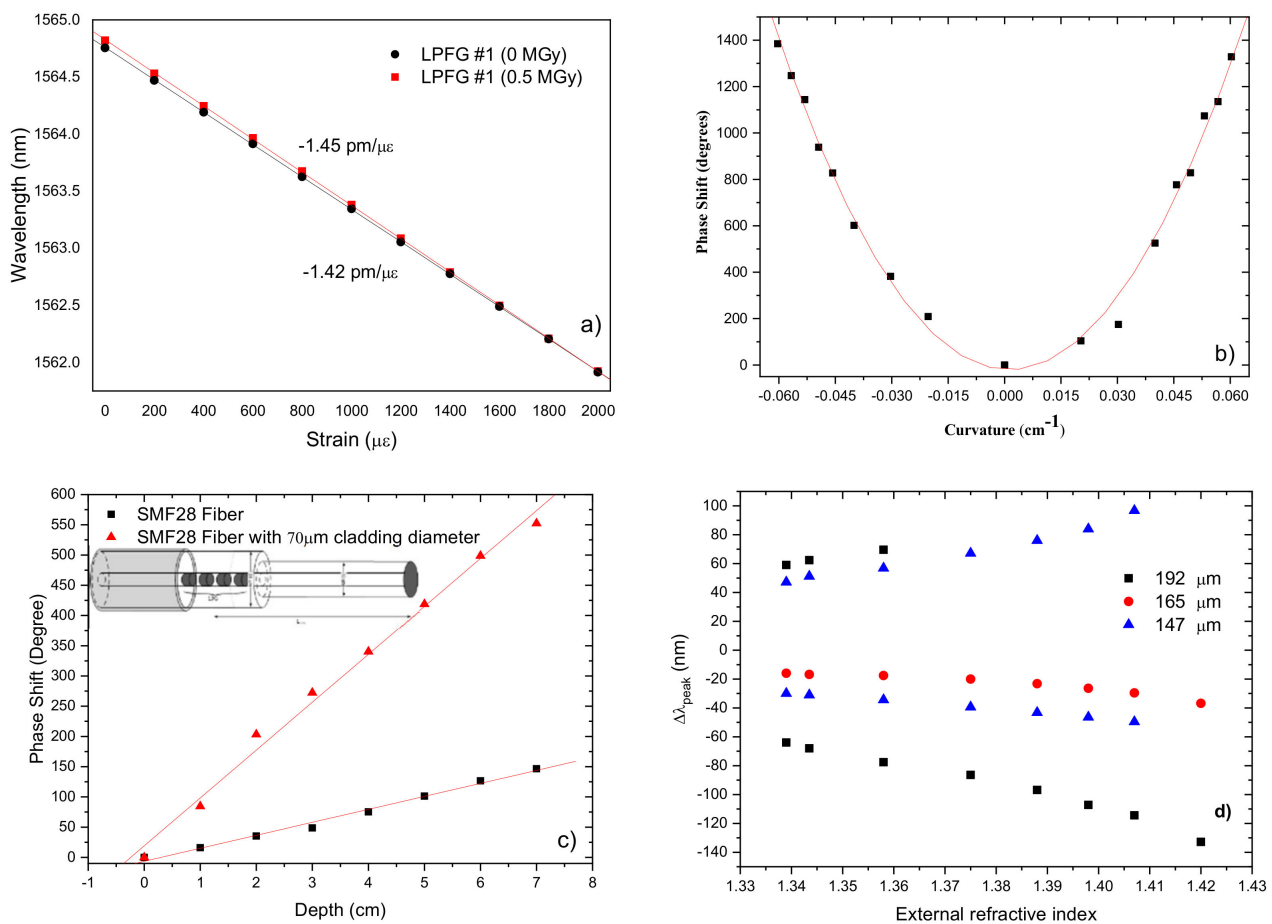


Figure 14. Characterization of LPFGs sensitivity to (a) Strain. Adapted with permission from [94] © 2021 The Optical Society; (b) bending. Reprinted with permission from [125]. © 2021 The Optical Society; (c) liquid level. Adapted with permission from [126] © 2021 SPIE; and (d) surrounding refractive index. Reprinted with permission from [127] © 2021 IEEE.

3.3. Polarization Dependence Loss

In our fabrication setup the arc discharge is directional, originating a temperature gradient that will cause asymmetric microdeformations in the fiber cladding and core. Since the perturbation is asymmetric, coupling occurs to asymmetric cladding modes and the gratings are intrinsically birefringent, that is, they possess polarization dependence loss [81,87,146]. Figure 15 shows a resonance dip and the corresponding PDL for two orthogonal polarizations. The dip separation is of about 1 nm and the PDL value is near 9 dB. In general, PDL values increase with the increase of the resonance loss, that is, the larger the asymmetric perturbation the larger the PDL values. Lower values or no use of external pulling tension leads to lower PDL values. The same also occurs for symmetric perturbations. In addition to the use of π -shifted Sagnac loop interferometer [147], the rotation of the fiber by 180° between discharges was also suggested for PDL reduction [148]. By following the latter procedure results are in general better however, they are as good as for the conventional technique under certain conditions (namely, low pulling tension) (Figure 16). It is expected that further improvement may be achieved if the fiber is, prior to each discharge, rotated by $360/n$, where n is the total number of arc discharges applied for the grating inscription.

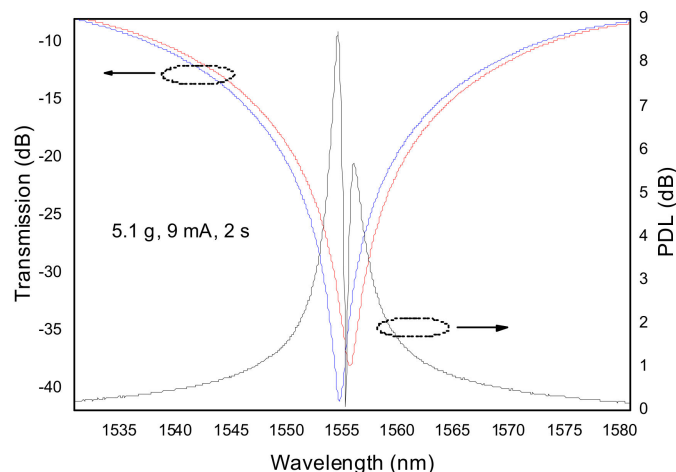


Figure 15. Transmission loss of LP_{14} resonance and respective PDL, inscribed using the following set of fabrication parameters: 5.1 g, 9 mA, 2 s and 30. Adapted with permission from ref. [81]. © 2021 Elsevier.

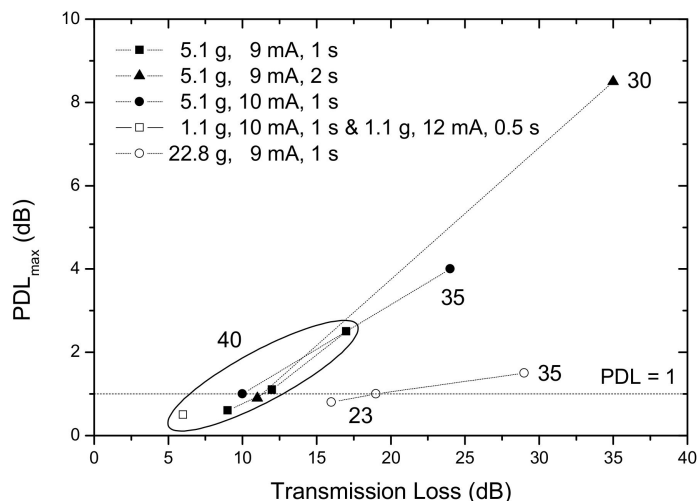


Figure 16. PDL values as a function of the transmission loss (LP_{14} cladding mode resonance) of several gratings produced under different fabrication parameters in the SMF28 fiber. Reprinted with permission from ref. [81]. © 2021 Elsevier.

3.4. Interactions with Uv-Radiation

In the early days several studies were conducted in order to study the interactions between uv-radiation and arc discharges. In fact, initially we would prefer to have knowledge on the changes that an arc discharge would cause to a fiber. For instance, we could make successive discharges along the fiber and afterwards write a fiber Bragg grating over it. The displacement of the Bragg wavelength in comparison to the one in a pristine fiber would give information on the core refractive index change caused by the arc discharge. Moreover, by writing tilted-FBGs on the pristine and arc-treated fiber, it is also possible to acquire information on the cladding refractive index change [149,150]. However, sooner was realized that the results would depend on the characteristics of the arc, the type of fiber, hydrogen loaded fiber and temperature annealing. In any case it was observed that after exposure of arc-induced gratings to uniform uv-radiation the spectrum would be almost completely erased. Afterwards if the fiber was properly annealed the spectrum would be almost fully recovered, although the resonance dips would be located at longer wavelengths. The change was attributed to a reaction of the hydrogen with the germanium doped silica matrix during the first annealing above 100 °C. It is interesting to note that for

both, Ge-doped and B/Ge co-doped fibers, the spectrum was recovered when a temperature coincident to the strain point was reached, 700 °C and 400 °C, respectively [96]. At this temperature starts the relaxation of elastic stresses and as will be discussed below that impacts the movement of the resonance dips. Nevertheless, the overall displacement towards longer wavelengths was larger than expected for just stress relaxation which means that some permanent refractive index change was caused by the uv-radiation. Figure 17 shows the evolution of the spectrum of a LPFG arc-induced in a B/Ge co-doped fiber while exposed to uniform uv-radiation and its afterwards recover while submitted to thermal annealing at 400 °C.

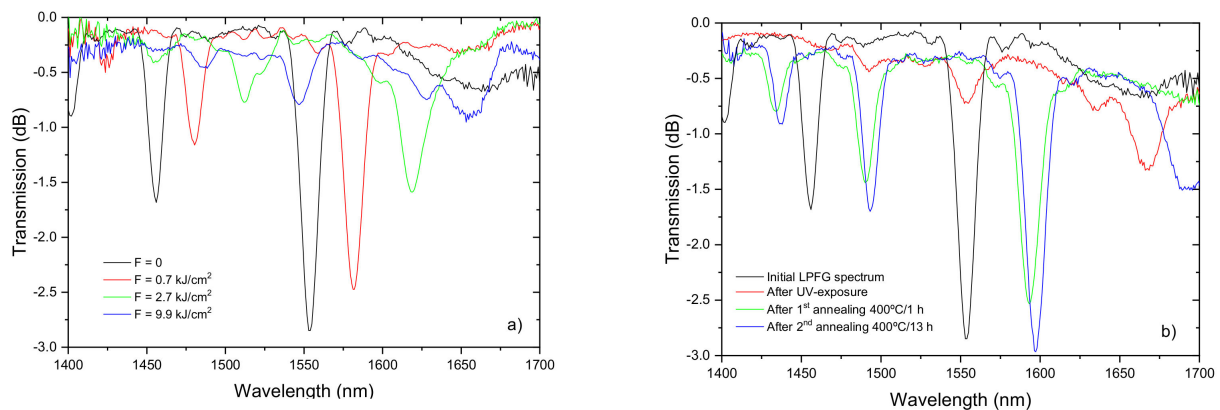


Figure 17. (a) Erasure of a LPFG arc-induced in a B/Ge co-doped fiber through uniform uv-radiation and (b) recover through thermal annealing. Reprinted with permission from ref. [96]. © 2021 Wiley Periodicals, Inc.

We have also demonstrated that a sampled FBG can be produced by fabricating a uv-induced FBG on top of an arc-induced grating and such a device was used to perform the simultaneous measurement of temperature and strain [151]. On the other hand, arc discharges can be applied to create, among other devices, apodised FBGs and Fabry-Perot filters [152].

3.5. Exposure to γ -Radiation

The effect of gamma radiation on arc-induced grating was also investigated [94]. It was demonstrated that total doses up to 0.5 MGy does not induces changes in the gratings spectra neither in their temperature and strain sensitivities (Figure 18). These results enable the possibility to use LPFGs arc-induced in pure-silica-core fibers, known as being a radiation-resistant optical fiber, for structural health monitoring of nuclear energy facilities.

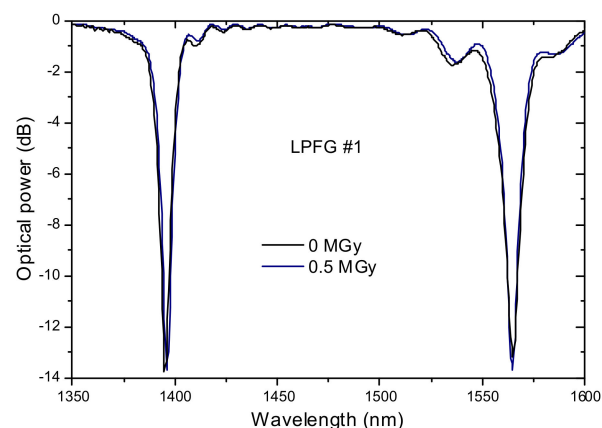


Figure 18. Effect of γ -radiation on an LPFG arc-induced in a pure-silica-core fiber. Adapted with permission from ref. [94]. © 2021 The Optical Society.

Recently, there is an increasing interest for this topic, since gratings arc-induced in non-radiation-resistant fibers can be used as radiation dosimeters [153–157].

4. Long-Period Fiber Gratings as Optical Fiber Sensors

In this section we will present three sensors for the simultaneous measurement of temperature and strain and also a flow sensor, based on the use of a LPFG or LPFG/FBG. As mentioned above LPFGs are very sensitive to physical parameters such as bending and in general there is cross sensitivity between two or more physical parameters. For instance, when measuring strain, the shift of the resonance wavelengths is also affected by temperature changes. Therefore, it is important to implement sensors able to measure simultaneously more than one parameter. This can be easily achieved by monitoring more than one resonance of a single LPFG since they exhibit different sensitivities to physical parameters. In general, the higher the order of the cladding mode resonance the higher the sensitivity. The problem is that resonances can be hundreds of nanometers away from each other and, therefore, two optical sources are required. There are several ways to overcome the issue, for instance, by using gratings with different periods having close resonances or having a grating inscribed in two dissimilar fibers. We have proposed three different approaches that enable the fabrication of a compact sensor in a single fiber requiring a single optical source: a sampled FBG, a step-changed LPFG and a dual LPFG inscribed in a B/Ge co-doped fiber. All schemes show neighbor resonances having different sensitivities to temperature and strain.

4.1. Sampled Fiber Bragg Grating

This sensor comprises the fabrication of a UV-induced FBG on top of an arc-induced LPFG [151]. After the inscription in a Corning dispersion-shifted fiber of a 25 mm-long LPFG with a period of 619 μm , the fiber was hydrogen loaded. Subsequently a 10 mm-long FBG was written over the LPFG using 248 nm radiation from a KrF laser through a uniform phase mask with a period of 538 nm. Since the arc discharge periodically modifies the core effective refractive index, the result is the growth of a sampled FBG exhibiting different resonance wavelengths [158]. Figure 19 shows the transmission and reflection spectrum of this sensor. As it can be seen the spectrum of the sampled FBG possess resonance wavelengths that stand in the different slopes of a higher order resonance of the LPFG. Since the temperature and strain sensitivity of both gratings is different, it was possible to convert the wavelength changes in optical power changes. Thus, a cheaper sensor head was developed, where optical power fluctuations were also compensated, and presented rms resolutions of ± 0.32 $^{\circ}\text{C}$ and ± 5.4 $\mu\epsilon$. As a final remark, it should be mentioned that a systematic study is still open since the behavior of this assembly depend not only on the relative physical location of both gratings but also on the location of their resonance wavelengths.

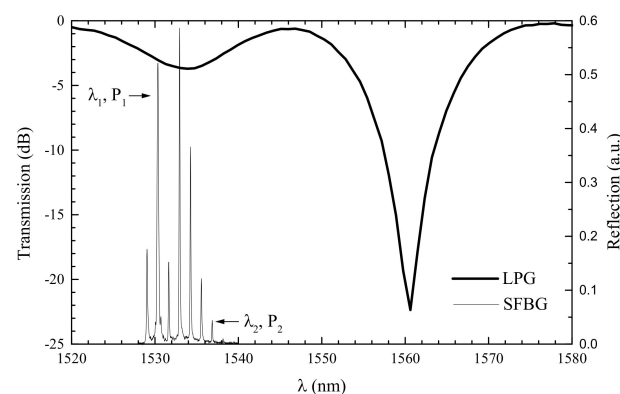


Figure 19. LPFG transmission spectrum and reflection spectrum of the sampled-FBG. Reprinted with permission from [151]. © 2021 IEE.

4.2. Step-Changed LPFG

Another interrogation scheme makes use of the fact that fabrication parameters of arc-induced gratings change not only the position of the resonance wavelengths but also their sensitivity. Thus, a first section of a 540 μm -LPFG was inscribed with the following fabrication parameters: $T = 22.8$ g, $I = 9$ mA, $t = 1$ s, $N = 15$ and afterwards they were modified during the inscription of the second section: $T = 1.2$ g, $I = 11$ mA, $t = 1$ s, $N = 40$, without any physical separation (Figure 20). This procedure resulted in a step-changed LPFG in which the spectrum exhibits two neighbour resonances in the third telecommunication window with different sensitivities to changes in temperature and strain, respectively $60.0/74.2$ pm/ $^{\circ}\text{C}$ and $-0.373/0.0$ pm/ $\mu\epsilon$. The *rms* deviations corresponding to temperature and strain were found to be ± 0.2 $^{\circ}\text{C}$ and ± 35 $\mu\epsilon$, respectively [159].

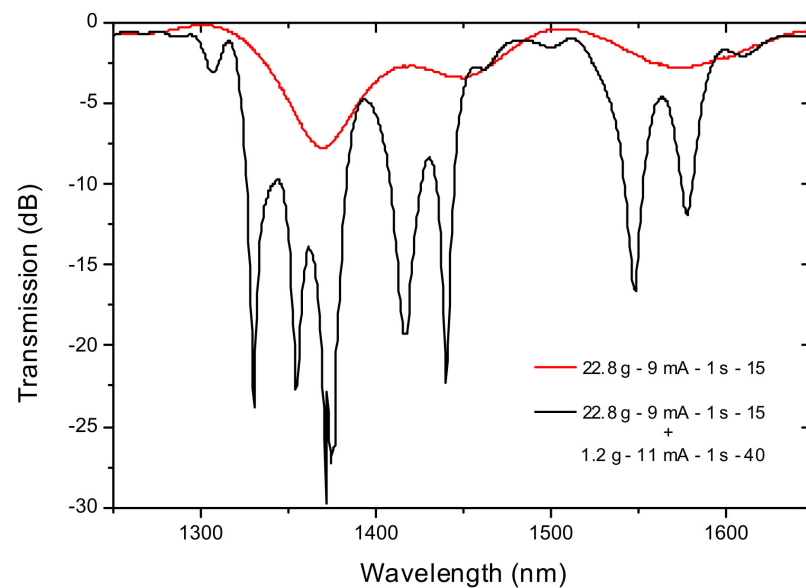


Figure 20. Evolution of the grating spectrum during the fabrication spectrum. Adapted from [86].

4.3. Dual Set of Resonances Corresponding to Different Formation Mechanisms

We have also proposed a new sensor based on the fact that under certain writing conditions it is possible to obtain in the B/Ge co-doped fiber a dual set of resonances belonging to distinct gratings. In fact, in this kind of fibers, LPFGs are typically arc-induced due to a densification mechanism being the coupling to symmetric cladding modes. However, when the arc discharge is directional and an external pulling tension is used during the grating inscription, the mechanism of formation in a standard fiber is due to microdeformations. Thus, by placing the fiber in a region where the temperature gradient is higher and the average temperature is lower we were able to increase the asymmetric mechanism to a level comparable to the symmetric one. Therefore, the transmission spectrum shows to neighbor resonances being the one at longer wavelengths due to densification and the other, at shorter wavelengths, due to microdeformations (Figure 21). We have demonstrated that through thermal annealing at high temperatures that the resonance at longer wavelengths vanishes [160]. The temperature and strain sensitivities of these resonances are, respectively, $-287/-289$ pm/ $^{\circ}\text{C}$ and $0.366/0.172$ pm/ $\mu\epsilon$ (Figure 22). Therefore, this sensor can perform temperature-compensated strain measurements.

4.4. Flow Sensor

The measurement of fluid velocity or flow is very important for instance to determine potential leaks of medicine gases in distribution pipes existing in health facilities. We have proposed an elegant flow sensor head comprising two gratings: a LPFG and a metal coated FBG [161]. The physical principle relies on heat transfer mechanisms, namely, convection. Basically, radiation from a pump laser, with 400 mW output power at 1480 nm, is injected

into the fiber and reaches a 385 μm -LPFG, arc-induced in the SMF28 fiber, which exhibits a coincident resonance wavelength. The radiation rejected by the resonance is afterwards absorbed by a 15 mm-long uniform silver thin film that overcoats a 10 mm-long FBG, with a Bragg wavelength centered at 1514 nm. A broadband source centered at 1550 nm is used to illuminate both gratings (Figure 23). Thus, as heat is absorbed by the film, its temperature increases and, therefore, the grating signature shifts towards longer wavelengths. Being the sensor head inserted in a test channel, air with increasing velocity flows through the channel and removes heat from the film, essentially, through convection and the Bragg wavelength shifts towards shorter wavelength following the decrease in temperature. The convection heat transfer coefficient depends on the fluid velocity and therefore a proper calibration enables the sensor to work as a flowmeter (Figure 24).

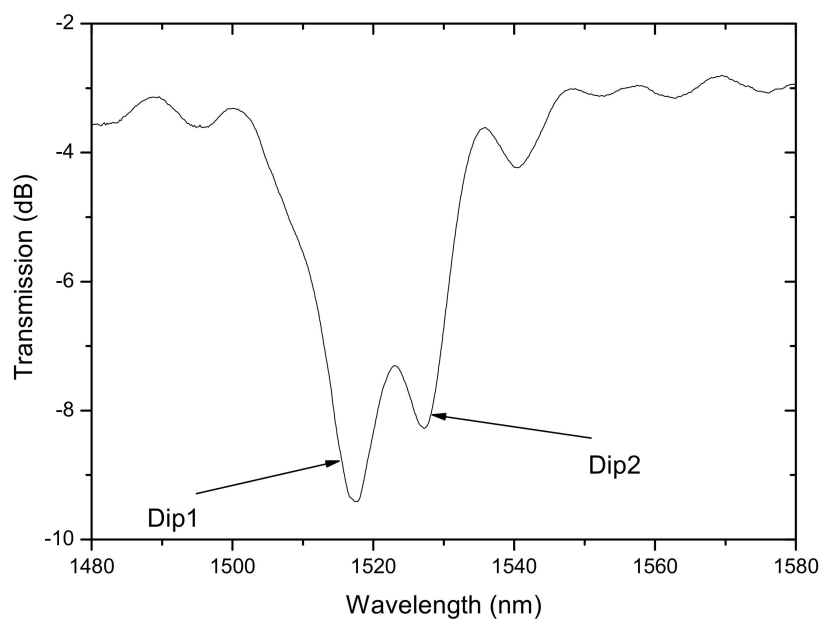


Figure 21. Dual resonances induced by different mechanisms in the B/Ge co-doped fiber. Reprinted with permission from [113]. © 2021 The Optical Society.

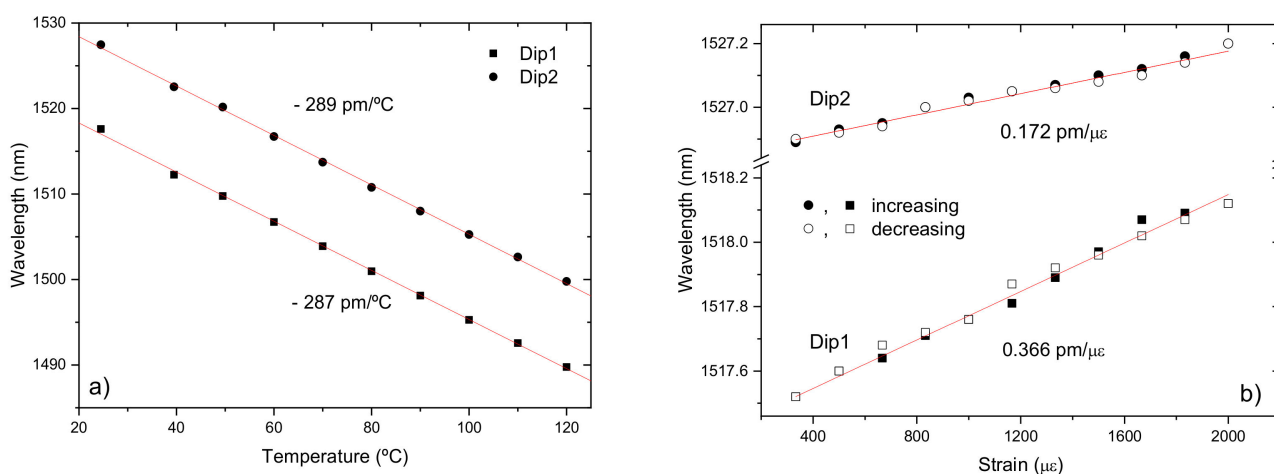


Figure 22. (a) Temperature and (b) strain sensitivities. Reprinted with permission from [113]. © 2021 The Optical Society.

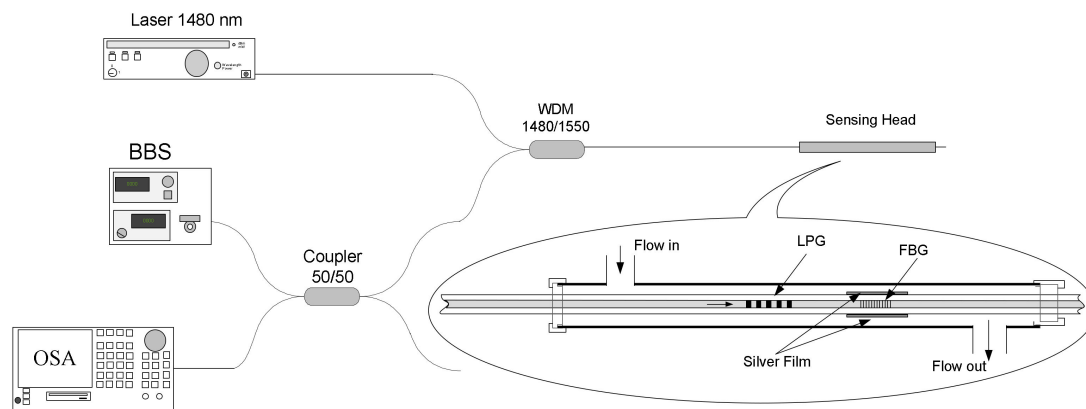


Figure 23. Experimental setup with detail of the sensing head. Reprinted with permission from [161]. © 2021 The Optical Society.

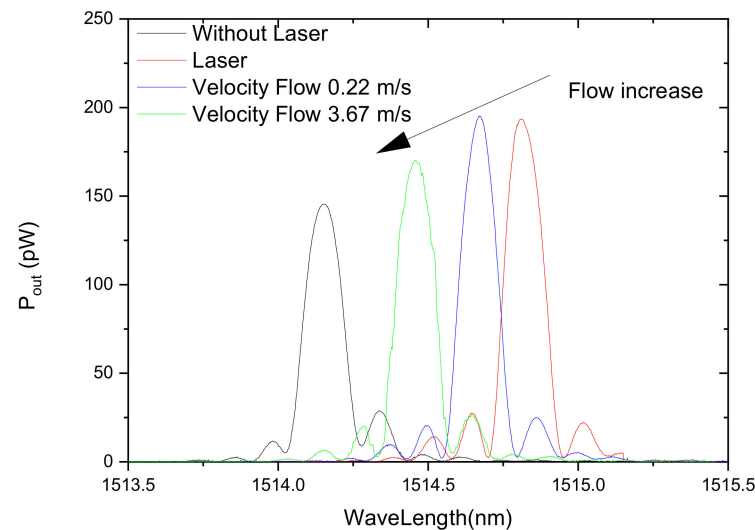


Figure 24. Response of the FBG Bragg wavelength as a function of air flow (laser on). Adapted with permission from [161]. © 2021 The Optical Society.

5. Conclusions

We have reviewed the most important achievements related to the properties and applications of arc-induced long-period fiber gratings. The thermal behavior of gratings was studied and some conclusions were drawn: gratings arc-induced in B/Ge co-doped fibers may find application at cryogenic temperatures due to their high temperature sensitivity; on the other hand, arc-induced gratings require proper annealing in order to be used at temperatures up to 1000 °C; long term use at high temperatures is limited due to potential fiber elongation, crystallization and core dopants diffusion. Gratings arc-induced in pure-silica-core fibers may find application in the monitoring of structural health in nuclear facilities. Interactions between arc discharges and uv-radiation enable the fabrication of several devices and to acquire knowledge on the changes caused by the discharges to the optical fiber. The polarization dependence loss was analyzed and identified as an intrinsic property that constitutes a drawback for most applications in optical communication domain. It was shown that the fabrication parameters can be used to tune the sensitivity of arc-induced gratings to changes in physical parameters. Several applications of LPGs as sensors, namely, for the simultaneous measurement of temperature and strain and also as flowmeters were presented. Arc-induced gratings may also find application as refractometric sensors based on the use of gratings in the turning points coated with thin films in the transition region.

Author Contributions: Conceptualization, methodology, writing—review and editing, G.R., O.V.I. and P.C. All authors have read and agreed to the published version of the manuscript.

Funding: This work was developed within the scope of the project proMetheus—Research Unit on Materials, Energy and Environment for Sustainability, FCT Ref. UID/05975/2020, financed by national funds through the FCT/MCTES. This work was also financed by National Funds through the Portuguese funding agency, FCT-Fundação para a Ciência e a Tecnologia, within project UIDB/50014/2020. O.V. Ivanov acknowledges support from the Russian Ministry of Higher Education and Science (project 075-15-2021-581).

Conflicts of Interest: The authors declare no conflict of interest.

References

1. Jiao, K.; Shen, H.; Guan, Z.; Yang, F.; Zhu, R. Suppressing stimulated Raman scattering in kW-level continuous-wave MOPA fiber laser based on long-period fiber gratings. *Opt. Express* **2020**, *28*, 6048–6063. [[CrossRef](#)] [[PubMed](#)]
2. Rao, Y.; Zhu, T.; Ran, Z.; Wang, Y.; Jiang, J.; Hu, A. Novel long-period fiber gratings written by high-frequency CO₂ laser pulses and applications in optical fiber communication. *Opt. Commun.* **2004**, *229*, 209–221. [[CrossRef](#)]
3. Vengsarkar, A.M.; Pedrazzani, J.R.; Judkins, J.B.; Lemaire, P.J.; Bergano, N.S.; Davidson, C.R. Long-period fiber-grating-based gain equalizers. *Opt. Lett.* **1996**, *21*, 336–338. [[CrossRef](#)] [[PubMed](#)]
4. Wsocki, P.F.; Judkins, J.B.; Espindola, R.P.; Andrejco, M.; Vengsarkar, A.M. Broad-band erbium-doped fiber amplifier flattened beyond 40 nm using long-period grating filter. *IEEE Photonics Technol. Lett.* **1997**, *9*, 1343–1345. [[CrossRef](#)]
5. Sohn, I.; Song, J. Gain flattened and improved double-pass two-stage EDFA using microbending long-period fiber gratings. *Opt. Commun.* **2004**, *236*, 141–144. [[CrossRef](#)]
6. Harumoto, M.; Shigehara, M.; Suganuma, H. Gain-flattening filter using long-period fiber gratings. *J. Lightwave Technol.* **2002**, *20*, 1027–1033. [[CrossRef](#)]
7. Rego, G. Optical filters for fiber lasers and amplifiers. *Microw. Opt. Technol. Lett.* **2008**, *50*, 890–894. [[CrossRef](#)]
8. Trifanov, I.; Caldas, P.; Neagu, L.; Romero, R.; Berendt, M.O.; Salcedo, J.A.R.; Podoleanu, A.G.; Lobo Ribeiro, A.B. Combined Neodymium—Ytterbium-doped ASE fiber-optic source for optical coherence tomography applications. *IEEE Photonics Technol. Lett.* **2011**, *23*, 21–23. [[CrossRef](#)]
9. Patrick, H.J.; Kersey, A.D.; Burns, W.K.; Moeller, R.P. Erbium-doped superfluorescent fibre source with long period fibre grating wavelength stabilisation. *Electron. Lett.* **1997**, *33*, 2061–2063. [[CrossRef](#)]
10. Ramachandran, S.; Yan, M.F.; Monberg, E.; Dimarcello, F.V.; Wisk, P.; Ghalmi, S. Record bandwidth, spectrally flat coupling with microbend gratings in dispersion-tailored fibers. *IEEE Photonics Technol. Lett.* **2003**, *15*, 1561–1563. [[CrossRef](#)]
11. Veeriah, S.; Faidz, A.R.; Phua, Y.N.; Mishra, V. Broadband spectrum based on mechanically induced cascaded long-period fibre gratings. *Microw. Opt. Technol. Lett.* **2005**, *44*, 463–465. [[CrossRef](#)]
12. Lin, C.Y.; Wang, L.A. A wavelength- and loss-tunable band-rejection filter based on corrugated long-period fiber grating. *IEEE Photonics Technol. Lett.* **2001**, *13*, 332–334. [[CrossRef](#)]
13. Chung, K.W.; Yin, S.Z. Analysis of a widely tunable long-period grating by use of an ultrathin cladding layer and higher-order cladding mode coupling. *Opt. Lett.* **2004**, *29*, 812–814. [[CrossRef](#)] [[PubMed](#)]
14. Dong, X.Y.; Yang, X.F.; Shum, P.; Chan, C.C. Tunable WDM filter with 0.8-nm channel spacing using a pair of long-period fiber gratings. *IEEE Photonics Technol. Lett.* **2005**, *17*, 795–797. [[CrossRef](#)]
15. Eom, T.J.; Kim, S.J.; Kim, T.Y.; Park, C.S.; Lee, B.H. Optical pulse multiplication and temporal coding using true time delay achieved by long-period fiber gratings in dispersion compensating fiber. *Opt. Express* **2004**, *12*, 6410–6420. [[CrossRef](#)] [[PubMed](#)]
16. Gu, X. Wavelength-division multiplexing isolation fiber filter and light source using cascaded long-period fiber gratings. *Opt. Lett.* **1998**, *23*, 509–510. [[CrossRef](#)]
17. Luo, H.; Sun, C.; Geng, T.; Yuan, L. A dark hollow beam generator based on special optical fiber with long period fiber grating. *Opt. Laser Technol.* **2021**, *134*, 106598. [[CrossRef](#)]
18. Zhou, M.; Zhang, Z.; Shao, L.; Liu, S.; Liu, Y.; Pang, Y.; Bai, Z.; Fu, C.; Cui, W.; Qi, L.; et al. Broadband tunable orbital angular momentum mode converter based on a conventional single-mode all-fiber configuration. *Opt. Express* **2021**, *29*, 15595–15603. [[CrossRef](#)]
19. Poole, C.D.; Presby, H.M.; Meester, J.P. 2-Mode Fiber Spatial-Mode Converter Using Periodic Core Deformation. *Electron. Lett.* **1994**, *30*, 1437–1438. [[CrossRef](#)]
20. Lee, K.S.; Erdogan, T. Transmissive tilted gratings for LP_{0,1}-to-LP₁₁ mode coupling. *IEEE Photonics Technol. Lett.* **1999**, *11*, 1286–1288.
21. Ortega, B.; Dong, L.; Liu, W.; deSandro, J.; Reekie, L.; Tsypina, S.; Bagratashvili, V.; Laming, R. High-performance optical fiber polarizers based on long-period gratings in birefringent optical fibers. *IEEE Photonics Technol. Lett.* **1997**, *9*, 1370–1372. [[CrossRef](#)]
22. Kopp, V.I.; Churikov, V.M.; Singer, J.; Chao, N.; Neugroschl, D.; Genack, A.Z. Chiral fiber gratings. *Science* **2004**, *305*, 74–75. [[CrossRef](#)]
23. Ramachandran, S.; Das, M.; Wang, Z.; Fleming, J.; Yan, M. High extinction, broadband polarisers using long-period fibre gratings in few-mode fibres. *Electron. Lett.* **2002**, *38*, 1327–1328. [[CrossRef](#)]

24. Lee, Y.W.; Jung, J.; Lee, B. Polarization-sensitive interference spectrum of long-period fiber grating pair separated by erbium-doped fiber. *IEEE Photonics Technol. Lett.* **2002**, *14*, 1312–1314.
25. Kim, C.S.; Han, Y.G.; Kang, J.U.; Choi, B.; Nelson, J.S. Polarization-insensitive multi-wavelength switching based on polarization-selective long-period fiber gratings. *Opt. Express* **2004**, *12*, 6082–6087. [[CrossRef](#)] [[PubMed](#)]
26. Kurkov, A.S.; Douay, M.; Duhem, O.; Leleu, B.; Henninot, J.F.; Bayon, J.F.; Rivoallan, L. Long-period fibre grating as a wavelength selective polarisation element. *Electron. Lett.* **1997**, *33*, 616–617. [[CrossRef](#)]
27. Bachim, B.L.; Ogunsola, O.O.; Gaylord, T.K. Optical-fiber-to-waveguide coupling using carbon-dioxide-laser-induced long-period fiber gratings. *Opt. Lett.* **2005**, *30*, 2080–2082. [[CrossRef](#)] [[PubMed](#)]
28. Kim, M.J.; Eom, T.J.; Paek, U.C.; Lee, B.H. Lens-free optical fiber connector having a long working distance assisted by matched long-period fiber gratings. *J. Lightwave Technol.* **2005**, *23*, 588–596.
29. Erdogan, T.; Stegall, D.; Heaney, A. Direct single-mode fiber to free space coupling assisted by a cladding mode. In Proceedings of the 1999 Optical Fiber Communications Conference, San Diego, CA, USA, 21–26 February 1999; pp. 171–173.
30. Perlin, V.; Winful, H. Nonlinear pulse switching using long-period fiber gratings. *J. Lightwave Technol.* **2000**, *18*, 329–333. [[CrossRef](#)]
31. Kutz, J.; Eggleton, B.; Stark, J.; Slusher, R. Nonlinear pulse propagation in long-period fiber gratings: Theory and experiment. *IEEE J. Sel. Top. Quantum* **1997**, *3*, 1232–1245. [[CrossRef](#)]
32. Kim, Y.; Kim, N.; Chung, Y.; Paek, U.; Han, W. All-optical switching application based on optical nonlinearity of Yb³⁺ doped aluminosilicate glass fiber with a long-period fiber gratings pair. *Opt. Express* **2004**, *12*, 651–656. [[CrossRef](#)] [[PubMed](#)]
33. Chiang, K.S.; Liu, Y.Q.; Ng, M.N.; Li, S.P. Coupling between two parallel long-period fibre gratings. *Electron. Lett.* **2000**, *36*, 1408–1409. [[CrossRef](#)]
34. Lauzon, J.; Chandonnet, A.; Xu, C.; Huang, W.P. Grating-assisted fused fibre filter. In Proceedings of the IOCC-ECOC 97—11th International Conference on Integrated Optics and Optical Fibre Communications/23rd European Conference on Optical Communications, Edinburgh, UK, 22–25 September 1997; Volume 2, pp. 169–172.
35. An, H.; Ashton, B.; Fleming, S. Long-period-grating-assisted optical add-drop filter based on mismatched twin-core photosensitive-cladding fiber. *Opt. Lett.* **2004**, *29*, 343–345. [[CrossRef](#)] [[PubMed](#)]
36. Kulishov, M.; Azana, J. Long-period fiber gratings as ultrafast optical differentiators. *Opt. Lett.* **2005**, *30*, 2700–2702. [[CrossRef](#)]
37. Stegall, D.; Erdogan, T. Dispersion control with use of long-period fiber gratings. *J. Opt. Soc. Am. A* **2000**, *17*, 304–312. [[CrossRef](#)]
38. Das, M.; Thyagarajan, K. Dispersion compensation in transmission using uniform long period fiber gratings. *Opt. Commun.* **2001**, *190*, 159–163. [[CrossRef](#)]
39. Han, Y.; Kim, C.; Kang, J.; Paek, U.; Chung, Y. Multiwavelength Raman fiber-ring laser based on tunable cascaded long-period fiber gratings. *IEEE Photonics Technol. Lett.* **2003**, *15*, 383–385.
40. Su, C.D.; Wang, L.A. Multiwavelength fiber sources based on double-pass superfluorescent fiber sources. *J. Lightwave Technol.* **2000**, *18*, 708–714. [[CrossRef](#)]
41. Romero, R.; Frazão, O.; Rego, G.; Marques, P.V.S.; Salgado, H.M. Sampled Fibre Bragg Gratings Fabrication using an Electric Arc and their Applications. In Proceedings of the 2002 Course on Photosensitivity in Optical Waveguides and Glasses, St. Petersburg, Russia, 17–21 June 2002.
42. Guo, B.; Guo, X.; Tang, L.; Yang, W.; Chen, Q.; Ren, Z. Ultra-long-period grating-based multi-wavelength ultrafast fiber laser [Invited]. *Chin. Opt. Lett.* **2021**, *19*, 071405. [[CrossRef](#)]
43. Silva-Alvarado, E.C.; Martinez-Rios, A.; Ledesma-Carrillo, L.M.; Jauregui-Vazquez, D.; Salceda-Delgado, G.; Porraz-Culebro, T.E.; Martin Vela, J.A.; Sierra-Hernandez, J.M. Switchable Ytterbium Fiber Laser Based on a Symmetrical Long-Period Fiber Grating. *IEEE Photonics J.* **2021**, *13*. [[CrossRef](#)]
44. Jiao, K.; Shen, H.; Yang, F.; Wu, X.; Bian, Y.; Zhu, R. Optimizing output spectral linewidth of fiber laser utilizing phase-shifted long-period fiber grating. *Opt. Laser Technol.* **2021**, *142*, 107221. [[CrossRef](#)]
45. Humbert, G.; Malki, A. High performance bandpass filters based on electric arc-induced pi-shifted long-period fibre gratings. *Electron. Lett.* **2003**, *39*, 1506–1507. [[CrossRef](#)]
46. Chen, L. Phase-shifted long-period gratings by refractive index-shifting. *Opt. Commun.* **2001**, *200*, 187–191. [[CrossRef](#)]
47. Starodubov, D.S.; Grubsky, V.; Feinberg, J. All-fiber bandpass filter with adjustable transmission using cladding-mode coupling. *IEEE Photonics Technol. Lett.* **1998**, *10*, 1590–1592. [[CrossRef](#)]
48. Choi, S.; Eom, T.J.; Jung, Y.; Lee, B.H.; Lee, J.W.; Oh, K. Broad-band tunable all-fiber bandpass filter based on hollow optical fiber and long-period grating pair. *IEEE Photonics Technol. Lett.* **2005**, *17*, 115–117. [[CrossRef](#)]
49. Han, Y.G.; Kim, S.H.; Lee, S.B.; Paek, U.C.; Chung, Y. Development of core mode blocker with H-2-loaded Ge-B codoped fibres. *Electron. Lett.* **2003**, *39*, 1107–1108. [[CrossRef](#)]
50. Dimmick, T.E.; Satorius, D.A.; Burdige, G.L. All-fiber acousto-optic tunable bandpass filter. In Proceedings of the 2001 Optical Fiber Communications Conference, Anaheim, CA, USA, 17–22 March 2001; p. Paper WJ3.
51. Bhatia, V. Applications of long-period gratings to single and multi-parameter sensing. *Opt. Express* **1999**, *4*, 457–466. [[CrossRef](#)]
52. Bhatia, V.; Campbell, D.; Claus, R.O.; Vengsarkar, A.M. Simultaneous strain and temperature measurement with long-period gratings. *Opt. Lett.* **1997**, *22*, 648–650. [[CrossRef](#)]
53. Bhatia, V.; Campbell, D.K.; Sherr, D.; Dalberto, T.G.; Zabaronick, N.A.; TenEyck, G.A.; Murphy, K.A.; Claus, R.O. Temperature-insensitive and strain-insensitive long-period grating sensors for smart structures. *Opt. Eng.* **1997**, *36*, 1872–1876. [[CrossRef](#)]

54. Liu, Y.; Zhang, L.; Bennion, I. Fibre optic load sensors with high transverse strain sensitivity based on long-period gratings in B/Ge co-doped fibre. *Electron. Lett.* **1999**, *35*, 661–663. [[CrossRef](#)]
55. Patrick, H.J.; Chang, C.C.; Vohra, S.T. Long period fibre gratings for structural bend sensing. *Electron. Lett.* **1998**, *34*, 1773–1775. [[CrossRef](#)]
56. Wang, L.A.; Lin, C.Y.; Chern, G.W. A torsion sensor made of a corrugated long period fibre grating. *Meas. Sci. Technol.* **2001**, *12*, 793–799. [[CrossRef](#)]
57. Lee, B.H.; Liu, Y.; Lee, S.B.; Choi, S.S.; Jang, J.N. Displacements of the resonant peaks of a long-period fiber grating induced by a change of ambient refractive index. *Opt. Lett.* **1997**, *22*, 1769–1771. [[CrossRef](#)] [[PubMed](#)]
58. Shu, X.W.; Zhu, X.M.; Jiang, S.; Shi, W.; Huang, D.X. High sensitivity of dual resonant peaks of long-period fibre grating to surrounding refractive index changes. *Electron. Lett.* **1999**, *35*, 1580–1581. [[CrossRef](#)]
59. Patrick, H.; Kersey, A.; Bucholtz, F. Analysis of the response of long period fiber gratings to external index of refraction. *J. Lightwave Technol.* **1998**, *16*, 1606–1612. [[CrossRef](#)]
60. Kristensen, M.; Russell, J.; Gao, S.; Cook, K.; Canning, J. Improved Spectral Resolution of Long-Period Fiber Grating Sensors for Ultra-High Temperature Environments Using Narrow Interferences between Regenerated Gratings. In Proceedings of the Bragg Gratings, Photosensitivity, and Poling in Glass Waveguides, Barcelona, Spain, 27–31 July 2014.
61. Davis, D.D.; Gaylord, T.K.; Glytsis, E.N.; Mettler, S.C. Very-high-temperature stable CO₂-laser-induced long-period fibre gratings. *Electron. Lett.* **1999**, *35*, 740–742. [[CrossRef](#)]
62. Zhu, T.; Rao, Y.J.; Song, Y.; Chiang, K.S.; Liu, M. Highly sensitive temperature-independent strain sensor based on a long-period fiber grating with a CO₂-laser engraved rotary structure. *IEEE Photonics Technol. Lett.* **2009**, *21*, 543–545. [[CrossRef](#)]
63. Zhao, D.; Zhou, K.; Chen, X.; Zhang, L.; Bennion, I.; Flockhart, G.; MacPherson, W.; Barton, J.; Jones, J. Implementation of vectorial bend sensors using long-period gratings UV-inscribed in special shape fibres. *Meas. Sci. Technol.* **2004**, *15*, 1647–1650. [[CrossRef](#)]
64. Zhang, L.; Liu, Y.; Zhao, Y.; Wang, T. High Sensitivity Twist Sensor Based on Helical Long-Period Grating Written in Two-Mode Fiber. *IEEE Photonics Technol. Lett.* **2016**, *28*, 1629–1632. [[CrossRef](#)]
65. Pilla, P.; Trono, C.; Baldini, F.; Chiavaioli, F.; Giordano, M.; Cusano, A. Giant sensitivity of long period gratings in transition mode near the dispersion turning point: An integrated design approach. *Opt. Lett.* **2012**, *37*, 4152–4154. [[CrossRef](#)] [[PubMed](#)]
66. Villar, I.D.; Matias, I.R.; Arregui, F.J.; Lalanne, P. Optimization of sensitivity in Long Period Fiber Gratings with overlay deposition. *Opt. Express* **2005**, *13*, 56–69. [[CrossRef](#)]
67. Rees, N.; James, S.; Tatam, R.; Ashwell, G. Optical fiber long-period gratings with Langmuir-Blodgett thin-film overlays. *Opt. Lett.* **2002**, *27*, 686–688. [[CrossRef](#)] [[PubMed](#)]
68. Rego, G. A Review of Refractometric Sensors Based on Long Period Fibre Gratings. *Sci. World J.* **2013**, *2013*, 913418. [[CrossRef](#)] [[PubMed](#)]
69. Esposito, F.; Srivastava, A.; Sansone, L.; Giordano, M.; Campopiano, S.; Iadicicco, A. Label-Free Biosensors Based on Long Period Fiber Gratings: A Review. *IEEE Sens. J.* **2021**, *21*, 12692–12705. [[CrossRef](#)]
70. Falciai, R.; Mignani, A.; Vannini, A. Long period gratings as solution concentration sensors. *Sens. Actuators B-Chem.* **2001**, *74*, 74–77. [[CrossRef](#)]
71. Wang, Y.; Liu, Y.; Zou, F.; Jiang, C.; Mou, C.; Wang, T. Humidity Sensor Based on a Long-Period Fiber Grating Coated with Polymer Composite Film. *Sensors* **2019**, *19*, 2263. [[CrossRef](#)]
72. Wang, J. Surface plasmon resonance humidity sensor based on twisted long period fiber grating coated with tungsten disulfide film. *Optik* **2021**, *236*, 166616. [[CrossRef](#)]
73. Corres, J.M.; Matias, I.R.; Villar, I.d.; Arregui, F.J. Design of pH Sensors in Long-Period Fiber Gratings Using Polymeric Nanocoatings. *IEEE Sens. J.* **2007**, *7*, 455–463. [[CrossRef](#)]
74. Wei, X.T.; Wei, T.; Xiao, H.; Lin, Y.S. Terbium doped strontium cerate enabled long period fiber gratings for high temperature sensing of hydrogen. *Sens. Actuators B Chem.* **2011**, *152*, 214–219. [[CrossRef](#)]
75. Korposh, S.; Selyanchyn, R.; Yasukochi, W.; Lee, S.-W.; James, S.W.; Tatam, R.P. Optical fibre long period grating with a nanoporous coating formed from silica nanoparticles for ammonia sensing in water. *Mater. Chem. Phys.* **2012**, *133*, 784–792. [[CrossRef](#)]
76. DeLisa, M.P.; Zhang, Z.; Shiloach, M.; Pilevar, S.; Davis, C.C.; Sirkis, J.S.; Bentley, W.E. Evanescent wave long period fiber Bragg grating as an immobilized antibody biosensor. *Anal. Chem.* **2000**, *72*, 2895–2900. [[CrossRef](#)]
77. Tripathi, S.M.; Bock, W.J.; Mikulic, P.; Chinnappan, R.; Ng, A.; Tolba, M.; Zourob, M. Long period grating based biosensor for the detection of Escherichia coli bacteria. *Biosens. Bioelectron.* **2012**, *35*, 308–312. [[CrossRef](#)]
78. Chiavaioli, F.; Baldini, F.; Tombelli, S.; Trono, C.; Giannetti, A. Biosensing with optical fiber gratings. *Nanophotonics* **2017**, *6*, 663–679. [[CrossRef](#)]
79. Esposito, F.; Sansone, L.; Srivastava, A.; Baldini, F.; Campopiano, S.; Chiavaioli, F.; Giordano, M.; Giannetti, A.; Iadicicco, A. Long period grating in double cladding fiber coated with graphene oxide as high-performance optical platform for biosensing. *Biosens. Bioelectron.* **2021**, *172*, 112747. [[CrossRef](#)] [[PubMed](#)]
80. Bandyopadhyay, S.; Biswas, P.; Chiavaioli, F.; Dey, T.K.; Basumallick, N.; Trono, C.; Giannetti, A.; Tombelli, S.; Baldini, F.; Bandyopadhyay, S. Long-period fiber grating: A specific design for biosensing applications. *Appl. Opt.* **2017**, *56*, 9846–9853. [[CrossRef](#)]
81. Rego, G.M.; Santos, J.L.; Salgado, H.M. Polarization dependent loss of arc-induced long-period fibre gratings. *Opt. Commun.* **2006**, *262*, 152–156. [[CrossRef](#)]

82. Frazao, O.; Rego, G.; Araujo, F.; Ferreira, L.; Salgado, H.; Santos, J. *Simultaneous Measurement of Strain and Temperature Based on Polarization Loss Properties of Arc-Induced Long-Period Gratings*; SPIE: Santander, Spain, 2004; Volume 5502.
83. Vengsarkar, A.; Lemaire, P.; Judkins, J.; Bhatia, V.; Erdogan, T.; Sipe, J. Long-period fiber gratings as band-rejection filters. *J. Lightwave Technol.* **1996**, *14*, 58–65. [[CrossRef](#)]
84. Shu, X.; Zhang, L.; Bennion, I. Sensitivity characteristics of long-period fiber gratings. *J. Lightwave Technol.* **2002**, *20*, 255–266.
85. Rego, G.; Marques, P.V.S.; Santos, J.L.; Salgado, H.M. Arc-induced long-period gratings. *Fiber Integr. Opt.* **2005**, *24*, 245–259. [[CrossRef](#)]
86. Rego, G.M. *Arc-Induced Long-Period Fibre Gratings: Fabrication and Their Applications in Optical Communications and Sensing*; Porto University: Porto, Portugal, 2006.
87. Esposito, F.; Campopiano, S.; Iadicicco, A. Arc-Induced Long Period Gratings in Erbium-Doped Fiber. *IEEE Photonics J.* **2019**, *11*. [[CrossRef](#)]
88. Ranjan, R.; Esposito, F.; Iadicicco, A.; Campopiano, S. Arc-Induced Long Period Gratings in Phosphorus-Doped Fiber. *IEEE Photonics Technol. Lett.* **2017**, *29*, 611–614. [[CrossRef](#)]
89. Ranjan, R.; Esposito, F.; Iadicicco, A.; StAncAlie, A.; Sporea, D.; Campopiano, S. Comparative Study of Long-Period Gratings Written in Standard and Fluorine-Doped Fibers by Electric Arc Discharge. *IEEE Sens. J.* **2016**, *16*, 4265–4273. [[CrossRef](#)]
90. Humbert, G.; Malki, A. Characterizations at very high temperature of electric arc-induced long-period fiber gratings. *Opt. Commun.* **2002**, *208*, 329–335. [[CrossRef](#)]
91. Humbert, G.; Malki, A. Annealing time dependence at very high temperature of electric arc-induced long-period fibre gratings. *Electron. Lett.* **2002**, *38*, 449–450. [[CrossRef](#)]
92. Rego, G.; Okhotnikov, O.; Dianov, E.; Sulimov, V. High-temperature stability of long-period fiber gratings produced using an electric arc. *J. Lightwave Technol.* **2001**, *19*, 1574–1579. [[CrossRef](#)]
93. Rego, G.; Santos, J.L.; Marques, P.V.S.; Salgado, H.M. Study of the properties of arc-induced long-period gratings and Bragg Gratings in B/Ge doped fibers. In Proceedings of the Bragg Gratings, Photosensitivity and Poling in Glass Waveguides Conference, Monterey, CA, USA, 1–3 September 2003; pp. 121–123.
94. Rego, G.; Fernandez, A.F.; Gusarov, A.; Brichard, B.; Berghmans, F.; Santos, J.L.; Salgado, H.M. Effect of ionizing radiation on the properties of arc-induced long-period fiber gratings. *Appl. Opt.* **2005**, *44*, 6258–6263. [[CrossRef](#)] [[PubMed](#)]
95. Fleming, J.W. Sub Glass Transition Relaxation in Optical Fibers. In Proceedings of the Optical Fiber Communication Conference, Los Angeles, CA, USA, 22 February 2004.
96. Rego, G. Long-period gratings ARC-induced in B/Ge codoped fibers: Thermal behavior and uniform exposure to UV-radiation. *Microw. Opt. Technol. Lett.* **2008**, *50*, 68–71. [[CrossRef](#)]
97. Rego, G. Annealing of arc-induced gratings at high temperatures. *Electron. Lett.* **2009**, *45*, 972–974. [[CrossRef](#)]
98. Morishita, K.; Kaino, A. Adjusting resonance wavelengths of long-period fiber gratings by the glass-structure change. *Appl. Opt.* **2005**, *44*, 5018–5023. [[CrossRef](#)]
99. Rego, G.; Caldas, P.; Ivanov, O.; Santos, J.L. Investigation of the long-term stability of arc-induced gratings heat treated at high temperatures. *Opt. Commun.* **2011**, *284*, 169–171. [[CrossRef](#)]
100. Martins, R.; Caldas, P.; Teixeira, B.; Azevedo, J.; Monteiro, J.; Belo, J.H.; Araújo, J.P.; Santos, J.L.; Rego, G. Cryogenic Temperature Response of Reflection-Based Phase-Shifted Long-Period Fiber Gratings. *J. Lightwave Technol.* **2015**, *33*, 2511–2517. [[CrossRef](#)]
101. James, S.W.; Tatam, R.P.; Twin, A.; Bateman, R.; Noonan, P. Cryogenic temperature response of fibre optic long period gratings. *Meas. Sci. Technol.* **2003**, *14*, 1409–1411. [[CrossRef](#)]
102. Choi, D.; Kim, J.; Roh, S.; Lee, B.; Lee, Y.W. Highly-Sensitive and -Linear Cryogenic Temperature Response of Long-Period Fiber Gratings Written on B-Ge-Codoped Photosensitive Fiber. *Jpn. J. Appl. Phys.* **2012**, *51*, 092501. [[CrossRef](#)]
103. Rego, G.; Marques, P.V.S.; Salgado, H.M.; Santos, J.L. Simultaneous measurement of temperature and strain based on arc-induced long-period fibre gratings. *Electron. Lett.* **2005**, *41*, 60–62. [[CrossRef](#)]
104. Rego, G.; Caldas, P.; Ivanov, O.V.V. Arc-Induced Long-Period Fiber Gratings at INESC TEC. Part I: Fabrication, Characterization and Mechanisms of Formation. *Sensors* **2021**, *21*, 4914. [[CrossRef](#)] [[PubMed](#)]
105. Rego, G.; Falate, R.; Kalinowski, H.J.; Fabris, J.L.; Marques, P.V.S.; Salgado, H.M.; Santos, J.L. Simultaneous temperature and strain measurement based on arc-induced long-period fiber gratings. In Proceedings of the 17th International Conference on Optical Fibre Sensors. International Society for Optics and Photonics, Bruges, Belgium, 23–27 May 2005; pp. 679–682.
106. Rego, G. Simultaneous measurement of temperature and strain based on ARC-induced long-period fiber gratings. A case study. *Microw. Opt. Technol. Lett.* **2008**, *50*, 2472–2474. [[CrossRef](#)]
107. Zhang, Y.; Zhang, Y.; Wang, Z.; Fan, L.; Zhuo, Q. *High Sensitivity Strain Sensor Based on Curved LPG Fabricated in Eccentric Hollow-core Fiber*; SPIE: Kunming, China, 2021; Volume 11763.
108. Esposito, F.; Ranjan, R.; Campopiano, S.; Iadicicco, A. Arc-Induced Long Period Gratings from Standard to Polarization-Maintaining and Photonic Crystal Fibers. *Sensors* **2018**, *18*, 918. [[CrossRef](#)] [[PubMed](#)]
109. Falate, R.; Frazão, O.; Rego, G.; Ivanov, O.; Kalinowski, H.J.; Fabris, J.L.; Santos, J.L. Bend and Temperature Sensing with Arc-Induced Phase-Shifted Long-Period Fiber Grating. In Proceedings of the Optical Fiber Sensors, Cancun, Mexico, 23–27 October 2006; p. TuE43.
110. Ouyang, Y.; Guo, H.; Ouyang, X.; Xu, X.; Zhou, C.; Zhou, A. Highly Sensitive Two-Axis Bending Sensor Based on Arc-Induced Long Period Fiber Grating in Dual Side-Hole Fiber. *IEEE Photonics J.* **2018**, *10*, 1–9. [[CrossRef](#)]

111. Sunduck, K.; Gil Hwan, K.; Kyu-Jin, H.; Olena, M.; Kwani, L.; Sang Hyuck, K.; Je-Myung, J.; Sang Bae, L. Investigation of curvature sensitivity of arc-induced long-period fiber gratings inscribed in a pure silica photonic crystal fiber with two large air holes in the outer cladding region. In Proceedings of the 2009 14th OptoElectronics and Communications Conference, Hong Kong, China, 13–17 July 2009; pp. 1–2.
112. Delgado, F.; Bessa, A. Torsion-dependent spectral response of long-period fiber grating based on electric arc technique with axial rotation of the fiber. *Microw. Opt. Technol. Lett.* **2019**, *61*, 178–181. [[CrossRef](#)]
113. Caldas, P.; Rego, G.; Ivanov, O.V.; Santos, J.L. Characterization of the response of a dual resonance of an arc-induced long-period grating to various physical parameters. *Appl. Opt.* **2010**, *49*, 2994–2999. [[CrossRef](#)]
114. Sun, B.; Wei, W.; Liao, C.; Zhang, L.; Zhang, Z.; Chen, M.; Wang, Y. Automatic Arc Discharge-Induced Helical Long Period Fiber Gratings and Its Sensing Applications. *IEEE Photonics Technol. Lett.* **2017**, *29*, 873–876. [[CrossRef](#)]
115. Bock, W.J.; Chen, J.; Mikulic, P.; Eftimov, T.; Korwin-Pawłowski, M. Pressure sensing using periodically tapered long-period gratings written in photonic crystal fibres. *Meas. Sci. Technol.* **2007**, *18*, 3098–3102. [[CrossRef](#)]
116. Smietana, M.; Bock, W.J.; Chen, J.; Mikulic, P. Highly sensitive pressure sensor based on long-period gratings written in a boron co-doped optical fiber. *Meas. Sci. Technol.* **2010**, *21*, 5. [[CrossRef](#)]
117. Smietana, M.; Bock, W.J.; Mikulic, P.; Chen, J. Increasing sensitivity of arc-induced long-period gratings—pushing the fabrication technique toward its limits. *Meas. Sci. Technol.* **2010**, *22*, 015201. [[CrossRef](#)]
118. Rego, G.M.; Santos, J.L.; Salgado, H.M. Refractive index measurement with long-period gratings arc-induced in pure-silica-core fibres. *Opt. Commun.* **2006**, *259*, 598–602. [[CrossRef](#)]
119. Falate, R.; Frazao, O.; Rego, G.; Fabris, J.L.; Santos, J.L. Refractometric Sensor Based on a Phase-Shifted Long Period Fiber Grating. *Appl. Opt.* **2006**, *45*, 5066–5072. [[CrossRef](#)]
120. Esposito, F.; Ranjan, R.; Campopiano, S.; Iadicicco, A. Experimental Study of the Refractive Index Sensitivity in Arc-induced Long Period Gratings. *IEEE Photonics J.* **2017**, *9*, 1–10. [[CrossRef](#)]
121. Esposito, F.; Srivastava, A.; Sansone, L.; Giordano, M.; Campopiano, S.; Iadicicco, A. Sensitivity Enhancement in Long Period Gratings by Mode Transition in Uncoated Double Cladding Fibers. *IEEE Sens. J.* **2020**, *20*, 234–241. [[CrossRef](#)]
122. Martinez-Rios, A.; Monzon-Hernandez, D.; Torres-Gomez, I. Highly sensitive cladding-etched arc-induced long-period fiber gratings for refractive index sensing. *Opt. Commun.* **2010**, *283*, 958–962. [[CrossRef](#)]
123. Silva, C.; Coelho, J.M.P.; Caldas, P.; Frazão, O.; Jorge, P.A.S.; Santos, J.L. Optical fiber sensing system based on long-period gratings for remote refractive index measurement in aqueous environments. *Fiber Integr. Opt.* **2010**, *29*, 160–169. [[CrossRef](#)]
124. Esposito, F.; Srivastava, A.; Iadicicco, A.; Campopiano, S. Multi-parameter sensor based on single Long Period Grating in Panda fiber for the simultaneous measurement of SRI, temperature and strain. *Opt. Laser Technol.* **2019**, *113*, 198–203. [[CrossRef](#)]
125. Caldas, P.; Jorge, P.A.S.; Araújo, F.M.; Ferreira, L.A.; Rego, G.; Santos, J.L. Geometrical effects on the refractive index sensitivity of Mach-Zehnder fibre modal interferometers based on long-period gratings. *Meas. Sci. Technol.* **2009**, *20*. [[CrossRef](#)]
126. Caldas, P.; Jorge, P.; Araújo, F.M.; Ferreira, L.; Marques, M.; Rego, G.; Santos, J. Fiber modal Michelson interferometers with coherence addressing and heterodyne interrogation. *Opt. Eng.* **2008**, *47*, 044401.
127. Colaço, C.; Caldas, P.; Villar, I.D.; Chibante, R.; Rego, G. Arc-Induced Long-Period Fiber Gratings in the Dispersion Turning Points. *J. Lightwave Technol.* **2016**, *34*, 4584–4590. [[CrossRef](#)]
128. Smietana, M.; Szmids, J.; Korwin-Pawłowski, M.L.; Bock, W.J.; Grabarczyk, J. Application of diamond-like carbon films in optical fibre sensors based on long-period gratings. *Diam. Relat. Mater.* **2007**, *16*, 1374–1377. [[CrossRef](#)]
129. Smietana, M.; Korwin-Pawłowski, M.L.; Bock, W.J.; Pickrell, G.R.; Szmids, J. Refractive index sensing of fiber optic long-period grating structures coated with a plasma deposited diamond-like carbon thin film. *Meas. Sci. Technol.* **2008**, *19*, 085301. [[CrossRef](#)]
130. Smietana, M.; Myśliwiec, M.; Mikulic, P.; Witkowski, B.S.; Bock, W.J. Capability for fine tuning of the refractive index sensing properties of long-period gratings by atomic layer deposited Al₂O₃ overlays. *Sensors* **2013**, *13*, 16372–16383. [[CrossRef](#)]
131. Smietana, M.; Koba, M.; Mikulic, P.; Bock, W.J. Combined plasma-based fiber etching and diamond-like carbon nanooverlay deposition for enhancing sensitivity of long-period gratings. *J. Lightwave Technol.* **2016**, *34*, 4615–4619. [[CrossRef](#)]
132. Smietana, M.; Bock, W.J.; Mikulic, P. Effect of high-temperature plasma-deposited nano-overlays on the properties of long-period gratings written with UV and electric arc in non-hydrogenated fibers. *Meas. Sci. Technol.* **2013**, *24*. [[CrossRef](#)]
133. Debowska, A.K.; Smietana, M.; Mikulic, P.; Bock, W.J. High temperature nano-coated electric-arc-induced long-period gratings working at the dispersion turning point for refractive index sensing. *Jpn. J. Appl. Phys.* **2014**, *53*. [[CrossRef](#)]
134. Pilla, P.; Giordano, M.; Korwin-Pawłowski, M.L.; Bock, W.J.; Cusano, A. Sensitivity Characteristics Tuning in Tapered Long-Period Gratings by Nanocoatings. *IEEE Photonics Technol. Lett.* **2007**, *19*, 1517–1519. [[CrossRef](#)]
135. Smietana, M.; Bock, W.J.; Mikulic, P. Temperature sensitivity of silicon nitride nanocoated long-period gratings working in various surrounding media. *Meas. Sci. Technol.* **2011**, *22*, 115203. [[CrossRef](#)]
136. Simões, E.; Abe, I.; Oliveira, J.; Frazão, O.; Caldas, P.; Pinto, J.L. Characterization of optical fiber long period grating refractometer with nanocoating. *Sens. Actuators B Chem.* **2011**, *153*, 335–339. [[CrossRef](#)]
137. Coelho, L.; Viegas, D.; Santos, J.L.; Almeida, J.M.M.M.D. Enhanced refractive index sensing characteristics of optical fibre long period grating coated with titanium dioxide thin films. *Sens. Actuators B Chem.* **2014**, *202*, 929–934. [[CrossRef](#)]
138. Coelho, L.; Viegas, D.; Santos, J.L.; de Almeida, J.M.M.M. Detection of Extra Virgin Olive Oil Thermal Deterioration Using a Long Period Fibre Grating Sensor Coated with Titanium Dioxide. *Food Bioprocess Technol.* **2015**, *8*, 1211–1217. [[CrossRef](#)]

139. Coelho, L.; Viegas, D.; Santos, J.L.; de Almeida, J.M.M.M. Characterization of zinc oxide coated optical fiber long period gratings with improved refractive index sensing properties. *Sens. Actuators B Chem.* **2016**, *223*, 45–51. [[CrossRef](#)]
140. Coelho, L.; de Almeida, J.M.M.M.; Santos, J.L.; da Silva Jorge, P.A.; Martins, M.C.L.; Viegas, D.; Queirós, R. Aptamer-based fiber sensor for thrombin detection. *J. Biomed. Opt.* **2016**, *21*, 087005. [[CrossRef](#)] [[PubMed](#)]
141. Coelho, L.; Santos, J.L.; Viegas, D.; De Almeida, J.M.M.M. Fabrication and Characterization of Metal Oxide-Coated Long-Period Fiber Gratings. *J. Lightwave Technol.* **2016**, *34*, 2533–2539. [[CrossRef](#)]
142. Coelho, L.; Viegas, D.; Santos, J.L.; De Almeida, J.M.M.M. Optical sensor based on hybrid FBG/titanium dioxide coated LPFG for monitoring organic solvents in edible oils. *Talanta* **2016**, *148*, 170–176. [[CrossRef](#)] [[PubMed](#)]
143. Coelho, L.; Moreira, J.A.; Tavares, P.B.; Santos, J.L.; Viegas, D.; de Almeida, J.M.M.M. Monitoring of oxidation phases of copper thin films using long period fiber gratings. *Sens. Actuators A Phys.* **2017**, *253*, 69–74. [[CrossRef](#)]
144. Monteiro-Silva, F.; Santos, J.L.; De Almeida, J.M.M.M.; Coelho, L. Quantification of Ethanol Concentration in Gasoline Using Cuprous Oxide Coated Long Period Fiber Gratings. *IEEE Sens. J.* **2018**, *18*, 1493–1500. [[CrossRef](#)]
145. Coelho, L.C.C.; Dos Santos, P.S.S.; Jorge, P.A.D.S.; Santos, J.L.; De Almeida, J.M.M.M. Real-Time Early Warning Strategies for Corrosion Mitigation in Harsh Environments. *J. Lightwave Technol.* **2018**, *36*, 1152–1158. [[CrossRef](#)]
146. Kim, M.; Lee, D.; Hong, B.; Chung, H. Performance characteristics of long-period fiber-gratings made from periodic tapers induced by electric-arc discharge. *J. Korean Phys. Soc.* **2002**, *40*, 369–373.
147. Son, J.; Lee, M.-K.; Jeong, M.Y.; Kim, C.-S. Polarization Dependence Suppression of Optical Fiber Grating Sensor in a π -Shifted Sagnac Loop Interferometer. *Sensors* **2010**, *10*, 4373–4380. [[CrossRef](#)] [[PubMed](#)]
148. Delgado, F.d.S.; dos Santos, A.B. Reduction of intrinsic polarization dependence in arc-induced long-period fiber gratings. *J. Opt. Eng.* **2018**, *57*, 067105. [[CrossRef](#)]
149. Erdogan, T.; Sipe, J.E. Tilted fiber phase gratings. *J. Opt. Soc. Am. A* **1996**, *13*, 296–313. [[CrossRef](#)]
150. Dong, X.; Zhang, H.; Liu, B.; Miao, Y. Tilted fiber Bragg gratings: Principle and sensing applications. *Photonic Sens.* **2011**, *1*, 6–30. [[CrossRef](#)]
151. Frazão, O.; Romero, R.; Rego, G.; Marques, P.V.S.; Salgado, H.M.; Santos, J.L. Sampled fibre Bragg grating sensors for simultaneous strain and temperature measurement. *Electron. Lett.* **2002**, *38*, 693–695. [[CrossRef](#)]
152. Rego, G. Fibre optic devices produced by arc discharges. *J. Opt.* **2010**, *12*, 113002. [[CrossRef](#)]
153. Mesonero-Santos, P.; Fernández-Medina, A.; Coelho, L.C.C.; Viveiros, D.; Jorge, P.A.; Belenguer, T.; López Heredero, R. Effect of Low-Doses of Gamma Radiation on Electric Arc-Induced Long Period Fiber Gratings. *Sensors* **2021**, *21*, 2318. [[CrossRef](#)]
154. Stăncălie, A.; Sporea, D.; Neguț, D.; Esposito, F.; Ranjan, R.; Campopiano, S.; Iadicicco, A. Long Period Gratings in unconventional fibers for possible use as radiation dosimeter in high-dose applications. *Sens. Actuators A Phys.* **2018**, *271*, 223–229. [[CrossRef](#)]
155. Esposito, F.; Stăncălie, A.; Neguț, C.D.; Campopiano, S.; Sporea, D.; Iadicicco, A. Comparative Investigation of Gamma Radiation Effects on Long Period Gratings and Optical Power in Different Optical Fibers. *J. Lightwave Technol.* **2019**, *37*, 4560–4566. [[CrossRef](#)]
156. Stancalie, A.; Esposito, F.; Neguț, C.D.; Ghena, M.; Mihalcea, R.; Srivastava, A.; Campopiano, S.; Iadicicco, A. A new setup for real-time investigations of optical fiber sensors subjected to gamma-rays: Case study on long period gratings. *Sensors* **2020**, *20*, 4129. [[CrossRef](#)] [[PubMed](#)]
157. Esposito, F.; Srivastava, A.; Campopiano, S.; Iadicicco, A. Radiation effects on long period fiber gratings: A review. *Sensors* **2020**, *20*, 2729. [[CrossRef](#)]
158. Guan, B.O.; Tam, H.Y.; Tao, X.M.; Dong, X.Y. Simultaneous strain and temperature measurement using a superstructure fiber Bragg grating. *IEEE Photonics Technol. Lett.* **2000**, *12*, 675–677. [[CrossRef](#)]
159. Rego, G.; Falate, R.; Ivanov, O.; Santos, J.L. Simultaneous temperature and strain measurements performed by a step-changed arc-induced long-period fiber grating. *Appl. Opt.* **2007**, *46*, 1392–1396. [[CrossRef](#)]
160. Rego, G.; Ivanov, O.V. Two types of resonances in long-period gratings induced by arc discharges in boron/germanium co-doped fibers. *Opt. Lett.* **2007**, *32*, 2984–2986. [[CrossRef](#)]
161. Caldas, P.; Jorge, P.A.S.; Rego, G.; Frazão, O.; Santos, J.L.; Ferreira, L.A.; Araújo, F. Fiber optic hot-wire flowmeter based on a metallic coated hybrid long period grating/fiber Bragg grating structure. *Appl. Opt.* **2011**, *50*, 2738–2743. [[CrossRef](#)]